Analysis and characterisation of a closed-loop control system for laser cooling and trapping experiment

by

Opeolu Victory

Thesis submitted in partial fulfilment of the requirements for the degree
Master of Engineering: Electrical Engineering

in the faculty of Engineering

at the Cape Peninsula University of Technology

Supervisor: Dr. Kessie Govender

Bellville

March 10, 2020

Declaration

I, Opeolu Victory, declare that the contents of this thesis represent my own unaided work, and that the thesis has not previously been submitted for academic examination towards any qualification. Furthermore, it represents my own opinions and not necessarily those of the Cape Peninsula University of Technology.

Signed Date

Abstract

This research is aimed at analysing the performance of a closed-loop feedback system of an external cavity diode laser (ECDL) for a laser (Doppler) cooling and atom trapping experiment.

External cavity diode lasers (ECDL) are commonly used in laser cooling experiments involving rubidium atoms. The laser frequency is controlled by adjusting the cavity length and the diode current. Using feedback control method, the laser is locked to an appropriate rubidium transition using a saturation absorption spectroscopy (SAS) setup together with a proportional-integral-derivative (PID) controller.

At the CPUT Quantum Physics research group, we have a laser cooling and atom trapping experimental setup. This setup is a combination of multiple optical, electrical and mechanical components. We first analyse this system experimentally using test signals. By passing in basic test input signals, we were able to measure the system by identifying and extracting certain properties such as the resonant

frequency, the damping constant and transient response of the system. The results generated from the experimental analysis further enabled us to estimate the transfer function of the external cavity diode laser (ECDL).

We then analyse the feedback setup numerically using known parameters from the experiment, and estimated parameters from the experimental analysis. We do this by first getting the mathematical model of the laser and then solving the differential equation using Euler methods in Matlab. By numerically analysing this feedback system, we are able to understand its transient behaviour. We were also able to test the system for different test scenarios e.g. tests for various controller constants, system response to different disturbance types and so on.

The similarities observed between the experimental and numerical analysis provide a reliable framework for future improvements when developing the feedback system. Elements such as the integrator constants, disturbance magnitudes and so on can be evaluated using the developed numerical closed-loop system.

Acknowledgments

First, I will like to thank my supervisor, Dr. Kessie Govender from the Department of Electrical, Electronic, and Computer Engineering at the Cape Peninsula University of Technology. He has dedicated a great amount of time, effort and patience to guide me through this research project. For the opportunity, the extra engineering and physics classes, the motivational talks, and the free coffee, I say thank you. I have definitely become a better student and person under his tutelage.

I would also like to thank the members of the Quantum Physics Research Group at the Cape Peninsula University of Technology for their support. They created a very friendly and welcoming environment and were very helpful when I needed help with academic work.

The financial assistance of National Research Foundation towards this research is acknowledged. Please note that opinions expressed in this thesis and the conclusions arrived at, are those of the author, and are not necessarily to be attributed

to the National Research Foundation.

I also wish to express my sincere gratitude to my family for their love and support over the period of study. They have been there for me all the way through the good and the not so good.

Finally I would like to thank everyone who contributed both directly or indirectly to the to completing this project. To the Department of Mechanical Engineering (Mechatronics), colleagues, and friends, I say thank you.

Research Outputs

Opeolu, V., Govender, K., Wyngaard, A., Ouassini, N., De Jager, G., and Scarrot, J. (2017), "Analysis and Performance of a closed loop external cavity diode laser control system", *in The Proceedings of SAIP2017, the 62nd Annual Conference of the South African Institute of Physics, edited by Prof. Japie Engelbrecht (SU/2017), pp. 210 - 215.* ISBN: 978-0-620-82077-6. Available online at http://events.saip.org.za.

Govender, K., Wyngaard, A., Opeolu, V., Pentz, R. (2018), "Design, development and characterization of a magneto-optical trap for laser cooling of Rubidium atoms: a project at the Cape Peninsula University of Technology", *Poster presentation at the 63rd Annual Conference of the South African Institute of Physics (SAIP2018).*

Contents

Chapter 1

Introduction and Literature Review

1.1 Introduction

Control systems are a vital component of our everyday life. We can think of a control system as a system that can be used to control a certain variable (e.g. temperature of water in an electric kettle) or even control a sequence of events (e.g. a washing machine, where a sequence of events are triggered when a wash mode is selected) (Bolton, 2018). Feedback control in particular form a crucial part of the control engineering field (Goodwin et al., n.d.).

Consider an example of a feedback system that involves all of us - your body temperature. Assuming you are not ill, your body temperature remains almost

constant whether you find yourself in a hot or cold environment. This is because the human body has a form of a "temperature control system". When the temperature of the external environment increases, you sweat and when it decreases, you shiver and thus your body temperature is restored. The control system in this case aims to always keep the body temperature constant.

Another practical application of a feedback control system can be observed in a centrally heated home, where to control the temperature, a human stands close to the furnace's power switch with a thermostat to measure the temperature and then turn on/off, depending on the thermostat's reading. This is a crude form of feedback control as the human in this case acts as the controlling element and the thermostat as the feedback element. In a more advanced system, there is a controller that automatically switches the furnace on/off, depending on the measured thermostat value.

Feedback control systems is used across various science and technology disciplines and one of such is quantum technology. Quantum technology is a relatively new field of physics and engineering, utilising some properties of quantum mechanics (e.g. quantum entanglement, superposition and tunnelling) into practical applications such as quantum computing, quantum cryptography, quantum simulation, quantum imaging and so on (Love, 2017; Singh, 2008).

Quantum computing is a simple example of a practical application. Quantum

computing employs quantum bits, which are two states of an atomic system. They are referred to as quantum bits. They are similar to classical bits except in the quantum case, the system can be in a superposition of both 0 and 1.

Quantum systems however are still quite complicated. They are very sensitive to environment and external influences, making the atoms/qubits lose their coherence when they are in a superposition state and when this happens, there is loss of information.

At the Cape Peninsula University of Technology, quantum system applications such as quantum computing and quantum information processing are being investigated by a group physicists and engineers through the study of cold atoms[1] (i.e. temperatures around 273^0C). Cold atoms are created using a system of laser beams interacting with atoms (rubidium atoms in our case) in a magneto-optical trap (MOT). To successfully get cold atoms, a lot of precision measurement and control is required. The laser frequency has to be precisely controlled for cooling, and the data outputs recorded accurately. In this project, we focus on analysing the control system for the laser used (an external cavity diode laser) and a data acquisition system for the laser cooling and trapping experiments.

[1]**Quantum Physics Research Group - CPUT:** `www.cput.ac.za/academic/faculties/engineering/research/quantum_physics`

1.2 Background and literature review

This project requires a solid understanding of concepts in atomic physics and control engineering. This section discusses briefly the concepts and techniques required for the proposed research. More in-depth details will be provided in a later chapter.

1.2.1 Laser cooling and locking

Laser cooling, also known as Doppler cooling is a technique used for the cooling of samples of neutral atoms or ions (Salim et al., 2012; Preston, 1996). It involves illuminating a cloud of atoms under low pressure to three pairs of laser beams arranged orthogonally. In each pair, the laser beams are counter-propagating. Figure 1.1 shows an example of one such pair.

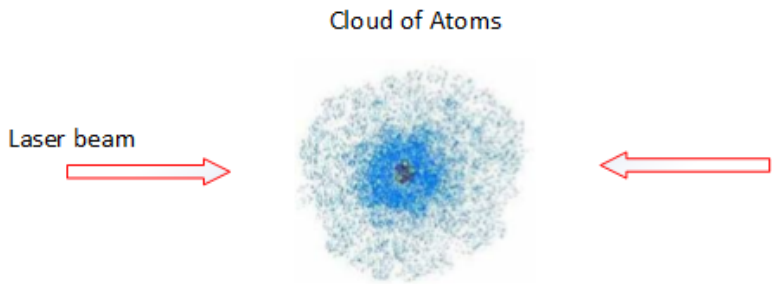

Figure 1.1: Laser interaction with cloud of atoms (Yahya, 2012).

Cooling is achieved by absorption and emission of the laser photons, which generates a velocity dependent force. Laser cooling involves the ability to cool a

sample of gas down to kinetic temperatures (e.g. $\sim 273^0C$) and confine them in a vacuum system over a period of time. For cooling to occur, the lasers have to be tuned to a very precise frequency and this is accomplished by using external cavity diode lasers and saturated absorption setup spectrometers (Salim et al., 2012). Figure 1.2 shows a general overview of a laser locking control model.

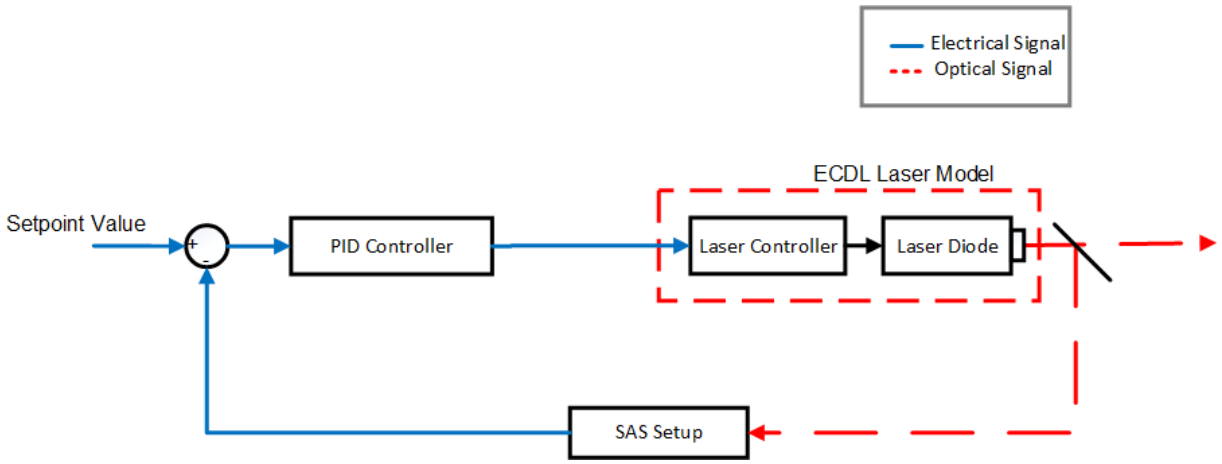

Figure 1.2: Overall block diagram of the laser control system

The system consists of a laser, a feedback scheme in form of a saturated absorption spectroscopy (SAS) setup and a proportional-integral-derivative (PID) controller (Weel et al., 2002). The aim is to keep the frequency of the laser locked on to a certain energy transition of the atoms (Dong et al., 2007). We further discuss below, the various blocks in figure 1.2.

External cavity diode lasers (ECDL)

Figure 1.3 shows a basic geometry of an external cavity diode laser (ECDL). It consists of a laser diode with a reflective coating on the rear surface and a reflection diffraction grating[2] mounted on a piezoelectric device.

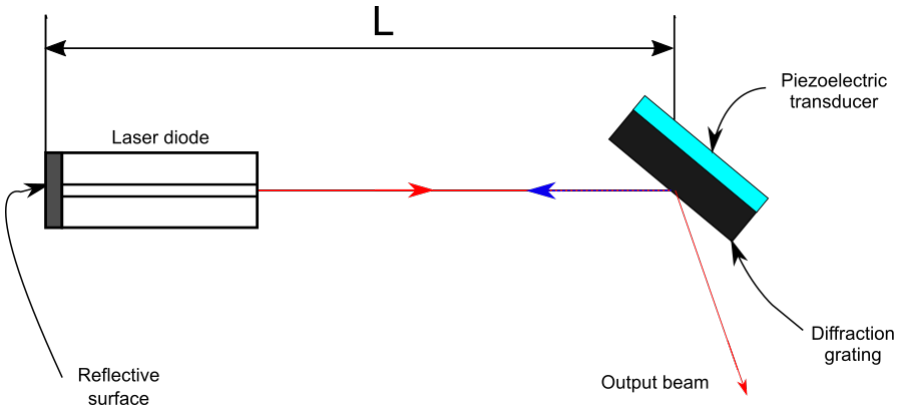

Figure 1.3: External cavity diode laser (ECDL) geometry

The laser diodes are generally inexpensive and available off the shelf. The output beam of the laser strikes the reflective diffraction grating, with one of the reflection orders directed back into the diode to form a cavity of length L as shown in figure 1.3. Another reflection order much weaker is reflected as the output beam.

The piezoelectric transducer (PZT) is ceramic actuator that converts electrical energy to mechanical energy by motion of very high resolutions (e.g.nanometer range deflection). By applying an input voltage signal to the piezo device, we can control the cavity length. Also, by applying a varying voltage to the piezo, we can

[2]a reflection diffraction grating operates as follows: when a laser beam strikes it, there are reflections at various angles, which we refer to as orders of reflection (Cunyun, 2004)

frequency modulate the laser output.

The resonant frequency of the cavity is given by:

$$F = cn/L \tag{1.1}$$

where c is the speed of light, n is an integer and L is the cavity length. Diode lasers are primarily developed for applications in wavelength division multiplexing (WDM) technology, coherent communication systems and sensing in precise measurements (Harvey et al., 1991).

Gawlik et al. (2004) elaborated on how critical precise control of the laser frequency is for laser cooling and trapping applications. The laser frequency however is not perfectly stable due to internal or external influences such as mechanical vibrations, air pressure, internal and external temperature variations etc. and these influences must be avoided to achieve a stable frequency (Weel et al., 2002; Cunyun, 2004; MacAdam et al., 1992).

Saturated absorption spectroscopy (SAS) setup (Feedback block)

The saturated absorption spectroscopy (SAS) block is used as the feedback element. It is used as a reference to measure the frequency of the laser beam. The input to this block (laser beam) is passed through a gas whose absorption spectra we know while the output of this block is an electrical signal from the photode-

tector. Depending on the laser frequency, the output will depend on where the laser frequency is on the absorption curve as seen in figure 1.4. The SAS setup is described in more detail in chapter 3.

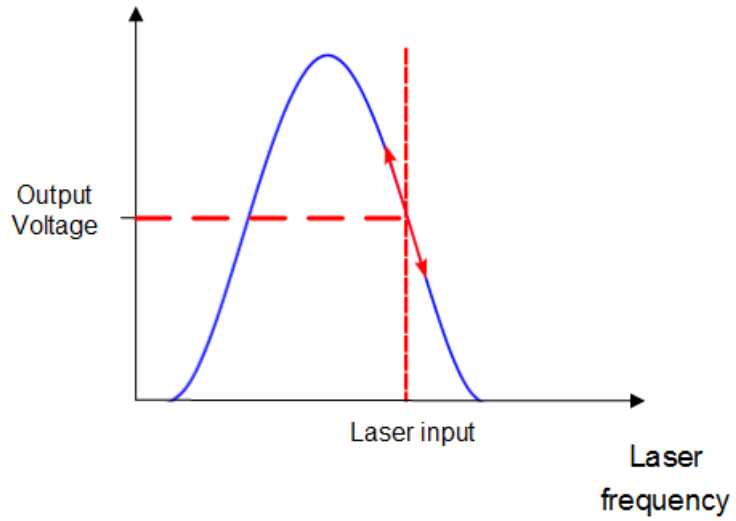

Figure 1.4: The known frequency response of the feedback block. The input to the feedback element is the laser frequency and the output is a voltage proportional to the input laser frequency

PID controller

PID control is the most commonly used control algorithm. The coefficients: Proportional(P), Integral(I), and Derivative(D) are varied to get the optimal response from a system. The difference between the setpoint value and the output of the saturated absorption spectroscopy setup (the difference/error signal) is determined. The error signal is amplified, integrated (and sometimes differentiated) before being fed to the piezoelectric device (Traptilisa, 2014; Nyamuda, 2006).

1.2.2 Research aims and objectives

The aim of this research is to investigate the behaviour and dynamics of the closed-loop control system used to lock the laser beam to a specific frequency. To successfully complete this research, the following objectives have been identified (these essentially form the chapters in this thesis)

1. Make a detailed study of the existing laboratory setup for laser locking.

2. Undertake a theoretical study of the basic ideas involved in this project.

3. Determine via experiments, the dynamic behaviour of the existing closed-loop system.

4. Conduct numerical simulation studies to obtain further insight into the behaviour of closed-loop ECDL control system.

1.2.3 Delineation of research

This research involves a number of people and is broken down into segments. The focus will be analysis of the control system used for laser trapping and cooling. It will not involve the setting up of the saturated absorption spectroscopy experiment and setting up the laser and optics will not be part of the project. Some experimental results however may be used for comparative analysis.

1.2.4 Thesis outline

Chapter 1 gives a broad overview of the concepts involved in this research with literature review.

In chapter 2, we discuss the description of the physical setup in the laboratory used to lock the laser frequency.

Chapter 3 discusses the basic ideas and theoretical concepts needed in more detail. They include control theory (e.g. feedback systems, transfer functions, etc) and the physics of laser atom interaction.

Chapter 4 discusses how we experimentally analysed the feedback control system. It explains our experimental operation modes, performance analysis and the results obtained (e.g. Transfer function of the closed-loop system).

In Chapter 5, we further analysed the closed-loop system numerically. We discuss how each component was modelled and simulated numerically in software. We also show the results for various test scenarios e.g. step response, system performance for various control constants and system response to different disturbance types.

Chapter 2

Physical Arrangement

2.1 Introduction

In this chapter, we describe the physical apparatus used in the laboratory to lock the laser frequency. We first show the overall feedback system block diagram and then we proceed to discuss how each component works and how they are interconnected.

2.2 System overview

Though we have given a simple illustration of a laser locking model in chapter 1, figure 2.1 shows a detailed control system as implemented in the laboratory.

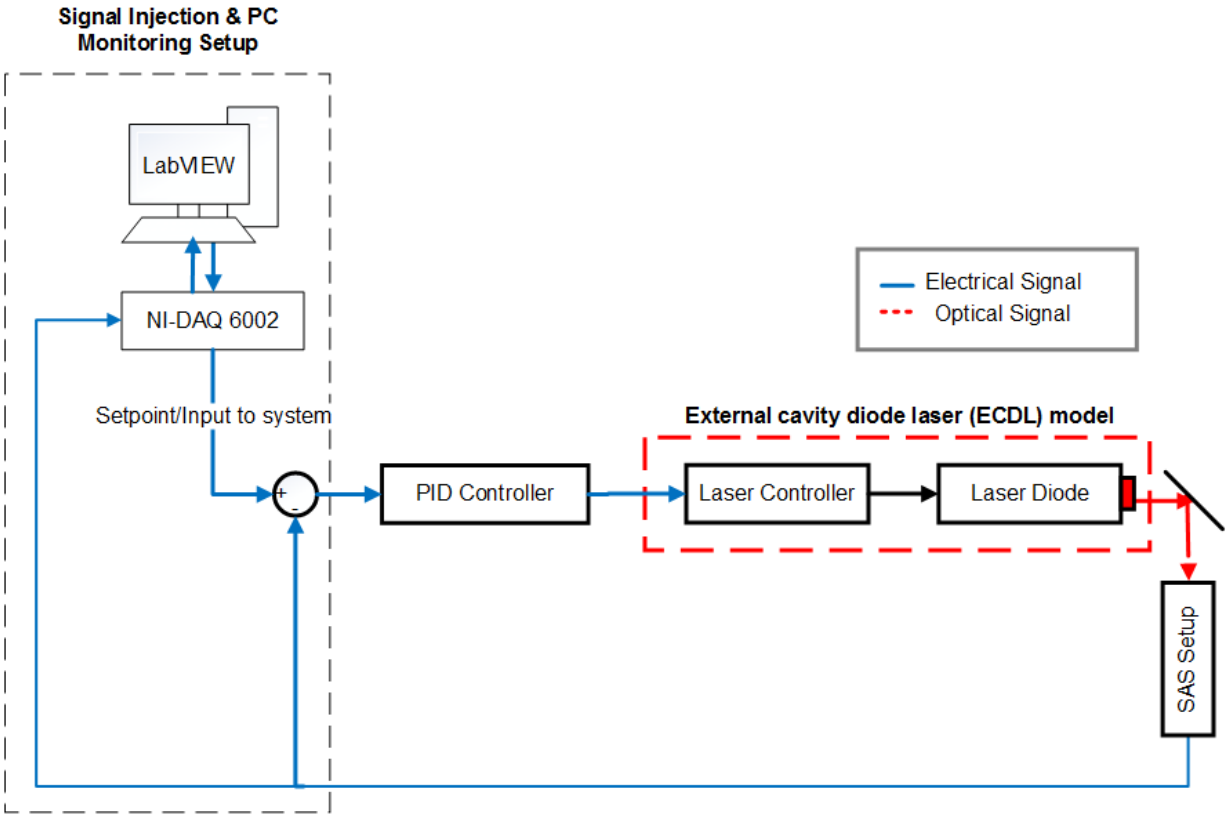

Figure 2.1: Block diagram of the laser locking control system

It consists of an external cavity diode laser (ECDL), a feedback setup in the form of a saturated absorption spectroscopy (SAS) experiment to measure the laser frequency, a proportional-integral-derivative (PID) controller and a PC monitoring/signal injection setup. The overall aim of this setup is to lock the laser frequency to a specific value and to monitor the performance of the entire closed loop system. A photograph of the entire apparatus is shown in figure 2.2.

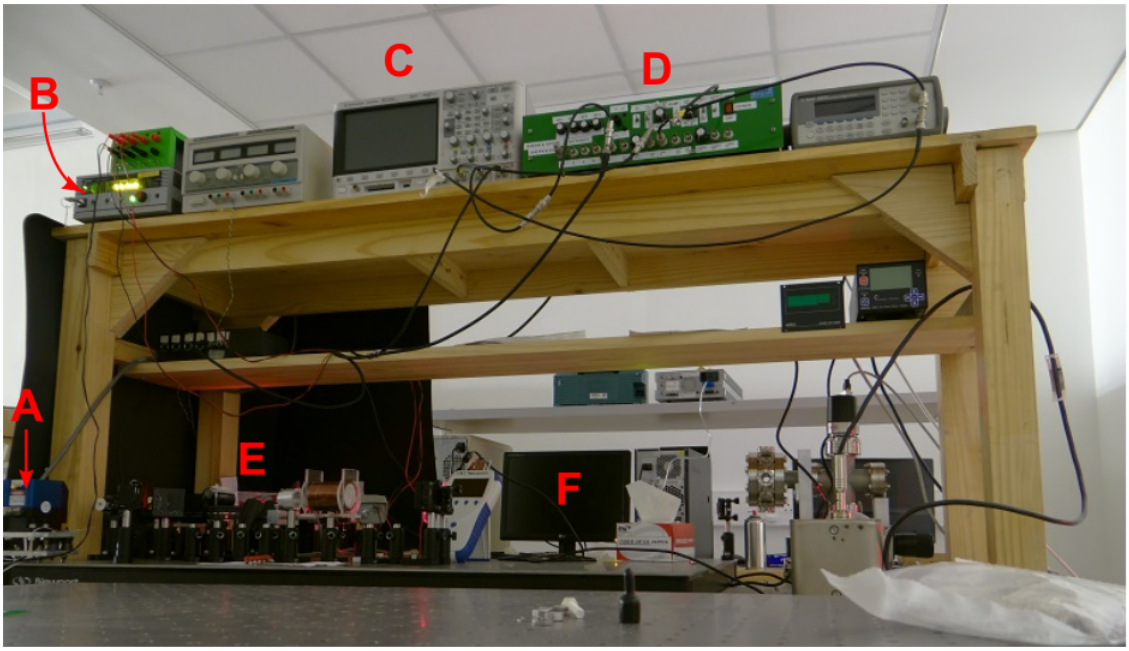

Where A - ECDL; B - Laser Controller; C - Oscilloscope;
D - PID Controller; E - Feedback (SAS) setup;
F - PC running LabVIEW

Figure 2.2: Experimental apparatus of our closed loop feedback system

Over the next few sections, we describe each of the components involved in the experimental setup.

2.2.1 External cavity diode laser (ECDL)

Figure 2.3 shows a basic geometry of an external cavity diode laser (ECDL). It consists of a laser diode with a reflective coating on the rear surface and a reflection diffraction grating. A reflection diffraction grating operates in a similar way to a mirror. The difference is how the light is reflected off the surface. When a laser

beam is strikes a reflection grating, the beam is reflected at multiple angles. The reflected beams are referred to as order of reflection (Hecht, 2013).

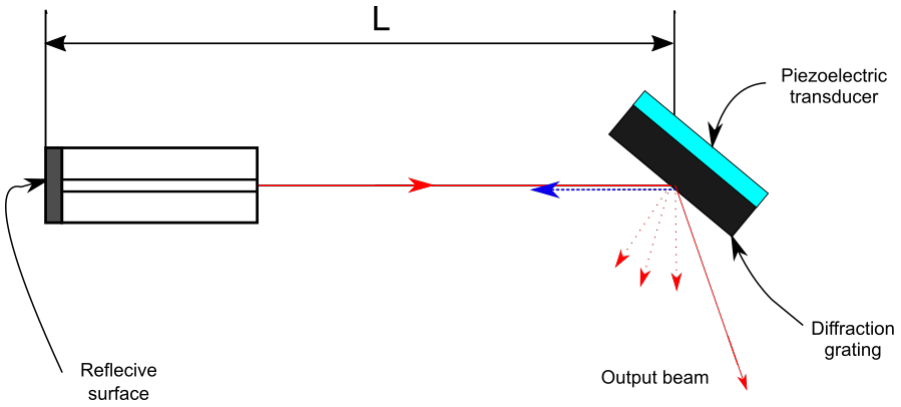

Figure 2.3: External cavity diode laser (ECDL) geometry

The output beam of the laser strikes the reflective diffraction grating, with one of the reflection orders directed back into the diode to form a cavity of length L as shown in figure 2.3. Another reflection order much weaker is reflected as the output beam. The diffraction grating is mounted on a piezoelectric transducer (PZT) as shown in figure 2.3. The piezoelectric transducer is ceramic actuator that converts electrical energy to mechanical energy by motion of very high resolutions (e.g. nanometer range deflection). By applying an input voltage signal to the piezo device, we can control the cavity length. The resonant frequency of the cavity is given by:

$$F = cn/L \tag{2.1}$$

where c is the speed of light, n is an integer and L is the cavity length.

By applying a varying voltage to the piezo, we can frequency modulate the laser output. For our experiments, we used the Vortex II TLB-6900 laser model which is a type of external cavity diode laser (ECDL). This is shown in figure 2.4.

Figure 2.4: Vortex II TLB-6900 External Cavity Diode Laser (Corporation, 2009)

The output frequency of the external cavity diode laser (ECDL), besides depending on the cavity length, also depends on the laser current. So the external cavity diode laser (ECDL) frequency can be controlled by both adjusting the cavity length and the laser current. The laser current gives us a finer control compared to the adjusting the cavity length.

2.2.2 Feedback block (SAS setup)

The purpose of this block is to determine the frequency of the laser beam. We do this by passing the laser through a gas sample, whose absorption spectra is known. By monitoring the intensity of the output beam from the gas sample, we can infer

where about on the absorption curve the beam is located. This is illustrated in figure 2.5.

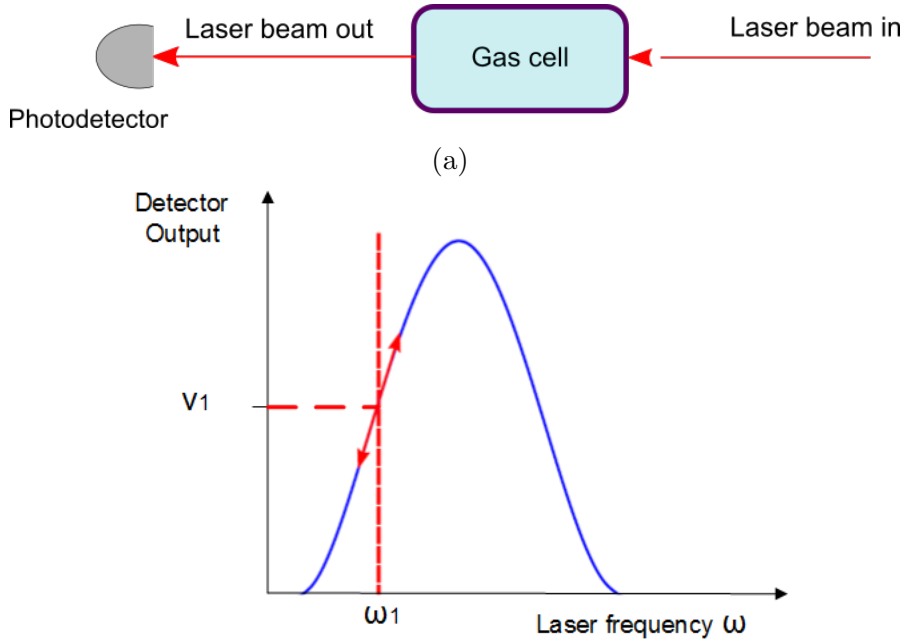

Figure 2.5: (a) Schematic of absorption measurement (b) frequency response of the gas sample.

If the laser beam frequency is ω_1, then the detector output will be v_1 for the situation shown in figure 2.5b.

The feedback block in the actual experiment essentially contains a setup similar to this except we have to take into account the fact that the atoms have thermal motion, which will cause broadening of the spectra. To counteract this broadening, we use a more complicated setup shown in figure 2.6

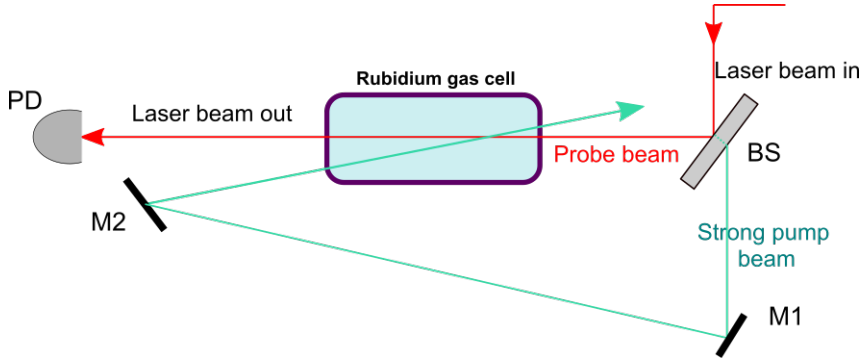

Figure 2.6: Schematic of a saturated absorption spectroscopy setup to determine the laser frequency

The detail explanation of how this setup works will be discussed in chapter 3. Figure 2.7 shows a photograph of the experimental setup, together with an overlay of the various beams.

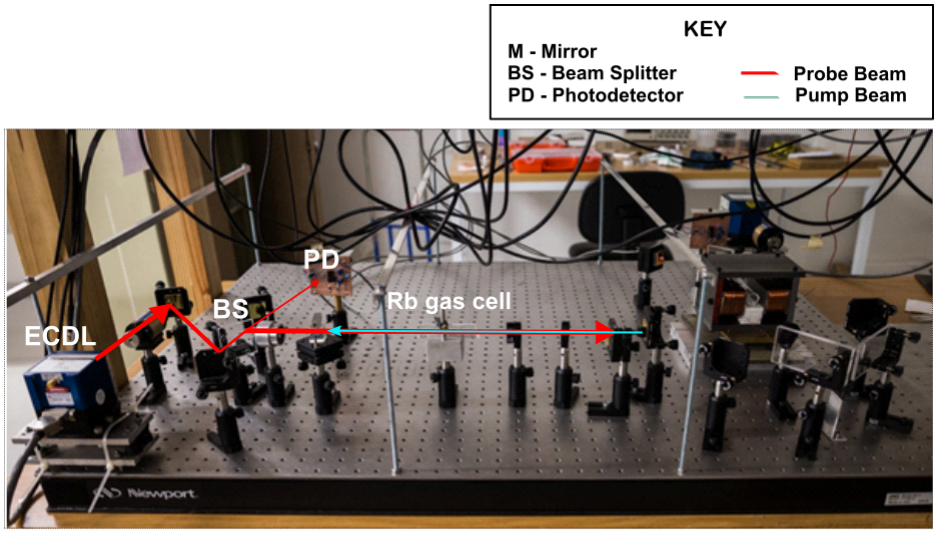

Figure 2.7: Saturated absorption spectroscopy laboratory setup

2.2.3 PI controller

The aim of this controller setup is to regulate and stabilize the frequency of the external cavity diode laser (ECDL) to a desired response. It compares the setpoint input signal with the feedback's output signal from the detector shown in figure 2.6, to derive the error signal. This error signal is then amplified, integrated (and sometimes differentiated) before being fed back to the piezoelectric device (Traptilisa, 2014; Nyamuda, 2006). The setup is illustrated by the diagram in figure 2.8.

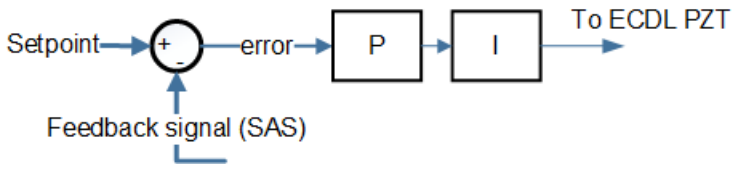

Figure 2.8: PI controller schematic

By varying the coefficients: proportional and integral, we are able to derive an optimal response of the laser frequency. Figure 2.9 shows the physical PID controller as set up at the laboratory.

Figure 2.9: PID controller box

Note that this controller was developed in house by another student and the

circuit diagram can be found in appendix A. More theoretical detail of control systems will be provided in chapter 3.

2.2.4 Data acquisition and setpoint control

The system to inject a setpoint signal and to measure the output laser frequency is shown in figure 2.10.

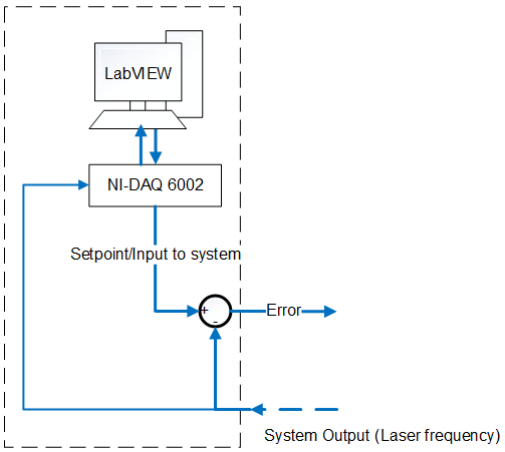

Figure 2.10: Schematic diagram of our data acquisition & setpoint control mechanism

The data acquisition (dashed section) consists of a PC running LabVIEW that is interfaced with a National Instruments data acquisition device (NI-6002 DAQ [1]). The NI-6002 generates (via the software) the setpoint and acquires the system output signal. We use various types of input signals. The signals used will be discussed further in chapter 4, where we discuss the experimental analysis.

[1] See appendix B for technical information.

2.3 Summary

We have described the laboratory setup of the laser locking feedback system. We have also discussed each component used in the experiment along with images where necessary. The control and atomic physics concepts used in the experiment will be discussed in more detail in the next chapter.

Chapter 3

Theory

3.1 Introduction

To successfully analyse the closed-loop feedback control of a atom trapping and laser cooling system, it is important to have a well grounded understanding of the two major concepts involved - control theory and atomic physics. In this chapter, we discuss in more detail concepts in control theory such as feedback systems, transfer functions and laser cooling concepts such as absorption, emission, etc.

3.2 Control theory

Control theory deals with the dynamic response of a system to commands and/or disturbances (Grantham et al., 1993). The aim of studying a dynamic system is

generally to gain an understanding of the system, with a view to controlling certain parameters.

To control a system, adjusting one or more inputs to the system is required. By adjusting the input, the system exhibits a transient response, followed by a steady-state behavior.

We take the heating of a room for example. The input in this case can be the voltage input to a power source and the output as the temperature of the room. However, there can also be heat flow from the environment that cannot be controlled. We refer to this input as a disturbance (Schwarzenbach et al., 1992). There are two broad classifications of control systems available - *open-loop systems* and *closed-loop control systems*

3.2.1 Open-loop and closed-loop control systems

With open-loop systems, the desired output of open-loop systems are generated based on prediction. This concept is illustrated in figure 3.1.

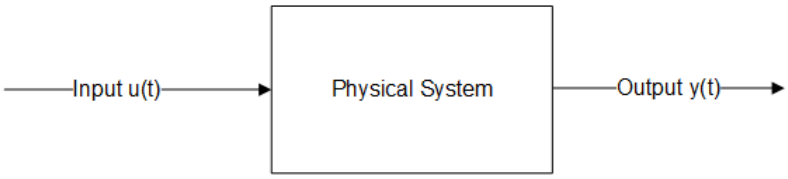

Figure 3.1: Open-loop control system

The inputs of an open-loop system does not depend explicitly on the output. Instead, they are generated using knowledge and information from past experience

of that system (Grantham et al., 1993). Such systems include washing machine, a boiler kettle etc.

The outputs of an open-loop system are sometimes undesirable as they can deviate due to unexpected disturbances to the system. A washing machine for example would only work perfectly as long as the water to soap to load weight ratio is perfectly proportional. The results change the moment any of the variable exceed a certain limit e.g. an increase in water pressure or load weight. This challenge is addressed with closed-loop feedback systems.

Closed-loop systems depend on the present state of the output, hence the need for a measuring device as shown in figure 3.2. The measurement from the output is called the feedback signal (Grantham et al., 1993; Bolton, 2018).

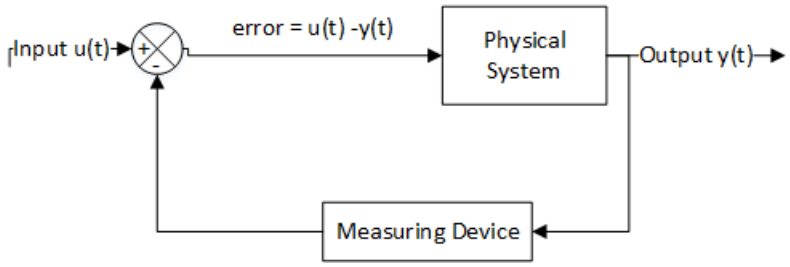

Figure 3.2: General closed-loop control system

With a closed-loop system, the output is first measured, then compared with the desired input (setpoint) and the system continually attempts to reduce the error between the setpoint and the measured system output. Closed-loop systems provide better performance and accuracy compared to open-loop systems as it provides the ability to control the transient and steady-state performance.

Using closed-loop control also has it's challenges. A system can become very unstable when delays for example occur in the loop. A slight delay in the flow from block to block can lead to corrective action applied late, therefore causing undercorrection or overcorrection. Thus we need to thoroughly analyse a system to develop optimal and efficient techniques to control the system (Dorf et al., 2000). Feedback system analysis is further discussed in the next sections.

3.2.2 Performance of feedback control systems

Early control systems such as James Watt's speed governor, a device to control the speed of steam engines, were developed with very little theoretical analysis (Schwarzenbach et al., 1992). However, as systems become more complex, with their performance requirements becoming more demanding, it has become necessary to resort to a more analytical approach. By analysing a system thoroughly, resources such as man power, time, money etc. are managed and allocated wisely.

Figure 3.3 shows an general overview of a feedback control system. It generally consists of the process to be controlled, sensors to detect these changes, a controller to compare the desired output with the measured output and implement the desired change with an actuator to activate or trigger the desired change to the plant.

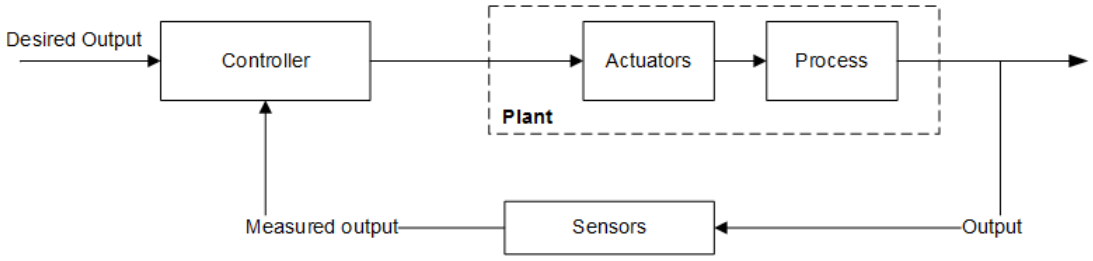

Figure 3.3: Feedback Control System (Phillips et al., 1995)

Feedback control systems are mainly used to reduce the effect of "uncertainty" in control systems (Phillips et al., 1995) . Uncertainty can be in the form of a modeling error in the unknown system (plant) or in the form of an unknown signal (disturbance).

Feedback control systems are inherently dynamic and as such, their performance is usually analysed and specified in terms of its transient response and its steady-state response.

The *transient response* is the response that occurs due to a change in input and disappears after a certain period of time. The *steady-state response* on the other hand is the response that remains after all transient responses have died down. Figure 3.4 gives a simple illustration of these concepts using a vertically suspended spring.

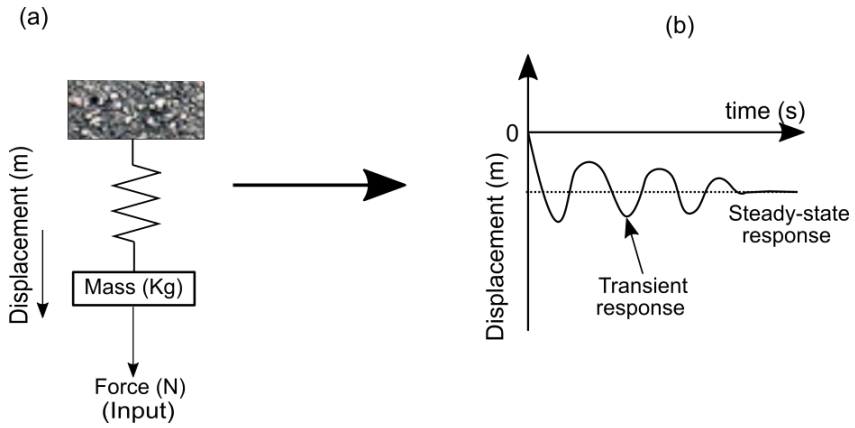

Figure 3.4: An simple illustration of a mass spring system, with its transient and steady-state response (b) (Bolton, 2018).

Assuming a force is suddenly applied to a mass-spring system which is in some equilibrium position, the spring then immediately stretches. The spring and mass oscillates at first and eventually settles down to a steady value. This steady value represents the steady-state response while the oscillation that occurs before it settles to a steady value is known as the transient response.

Analysing a control system helps in determining the details of the transient response and the final settling value, thereby observing the quality of its performance.

Test input signals

Using test input signals is an important part of analysing feedback control systems. We know an input signal produces a transient response when applied to a control system. The applied force from figure 3.4 on the mass-spring system is an example

of such input. During normal operation however, the input signals at various points in the system is dynamically varying, making it difficult to simulate them. To circumvent this, test input signals are generally used in control engineering. These test signals allows us to characterize the system for any types of input to the system.(Dorf et al., 2000; Burghes et al., 1980).

Test input signals generally used in control systems analysis include step input, ramp input & parabolic input as shown in figure 3.5. Using these test inputs, we are able to predict the response due to any other input signal. The step reference input for example is used in systems that may experience sudden changes (disturbances) at a certain point in time. Ramp as a reference input can also be used to follow gradually changing systems.

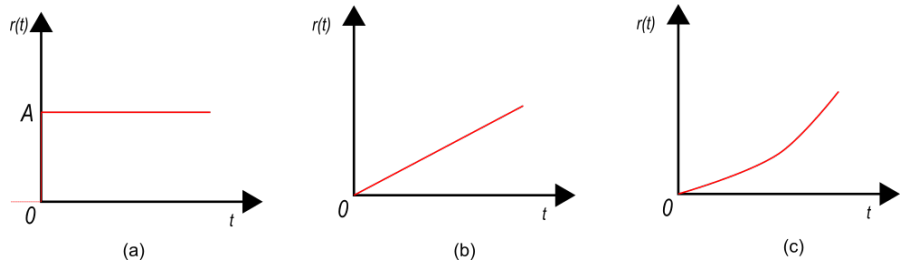

Figure 3.5: Test Input Signals (Dorf et al., 2000)

The ramp signal is the integral of the step input while the parabolic signal is the integral of the ramp input. Table 3.1 shows the equations representing the various test signals in the time and Laplace domain respectively.

Table 3.1: Test Signal Inputs

Test Signal	**r(t)**	**R(s)**
Step	$r(t) = A, t>0$ $= 0, t<0$	$R(s) = A/s$
Ramp	r(t)=At, t>0 $= 0$, t<0	$R(s) = A/s^2$
Parabolic	r(t)=At^2, t>0 $= 0$, t<0	$R(s) = 2A/s^3$

A unit impulse function is also sometimes used as a test signal. It is based on the limiting form of a rectangular function:

$$\left\{ \begin{array}{cc} \lim_{\epsilon \to 0} \frac{1}{\epsilon}, & \frac{-\epsilon}{2} \leq t \leq \frac{1\epsilon}{2} \\ 0 & \text{otherwise} \end{array} \right\}$$

Step input signal is the easiest to generate and evaluate and as such, primarily chosen for performance tests (Dorf et al., 2000). Standard performance measures are therefore generally analysed in terms of the step response of a system. Figure 3.6 shows an example when step test signals are applied to a practical system. Using the mass spring system in figure 3.4 as a reference, we assume the mass m of the object to be $1Kg$ and the spring constant k to be $1N/m$. In reality, we understand that the spring will not oscillate forever due to effects such as air

resistance or energy lost[1] in the spring. Instead, it will oscillate for a certain period, with the amplitude diminishing to an eventual state of rest. For this illustration, we assumed a frictional constant of $0.8Ns/m$

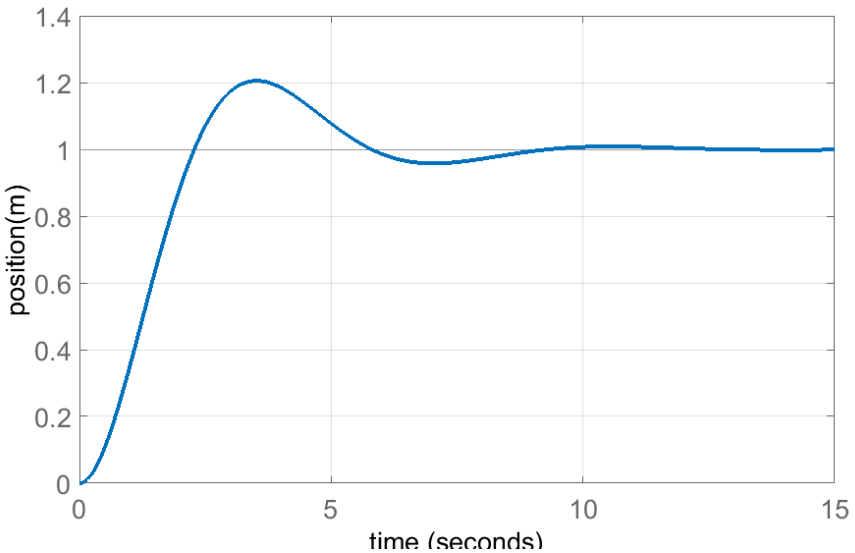

Figure 3.6: Step response example for a mass spring system.

By applying a step input force F of $1N$, a transient response was induced as seen in figure 3.6. Note that the system is analysed in the X-Y plane as we assume both the mass and spring are moving in the Y direction.

Transfer Functions

Transfer functions are used in control engineering to represent the relationship between the input and output of a system. It describes the dynamic characteristics

[1]Due to the law of conservation of energy, energy is not necessarily "lost". Instead, it is converted from mechanical energy to heat energy

of the system. According to Schwarzenbach et al., 1992, the transfer function of a linear system is defined as "the ratio of the Laplace transform of the output to the Laplace transform of the input when all initial conditions are zero". The transfer function is therefore represented by the general form:

$$G(s) \triangleq \frac{Y(s)}{X(s)} \tag{3.1}$$

where $Y(s) \rightarrow$ system output and $X(s) \rightarrow$ system input. $Y(s)$ and $X(s)$ are polynomials in s.

For a system to be physically realizable, it is important the order of the numerator not exceed that of the denominator (Morari et al., 1989). When a transfer function has a its zeroes greater than the number of poles, it creates pure differentiators. Pure differentiators suggest that the transfer function represents a system that is not casual i.e. it is not physically realizable.

From the transfer function, it is possible to assess the system behaviour. The dynamic system, usually represented by a differential equation is analysed and rewritten using Laplace transform notation. We consider a simple example in the mass-spring-damper system as seen in figure 3.7. It has three elements: a mass m measured in kg, a damping coefficient b and a spring constant k measured in N/m.

The mathematical model of this system is derived using Newton's second law of motion. It states that the sum of applied force us equal to the rate of change

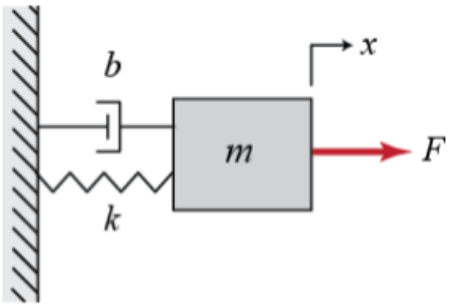

Figure 3.7: A simple mass-spring-damper system.

of momentum.

$$\sum F = f(t) - f_s(t) - f_d(t) = M\frac{d^2x}{dt^2} \tag{3.2}$$

The force produced by the spring $f_s = kx(t)$ and the damping force $f_d = b\frac{d^2x}{dt^2}$.

Rewriting Eq. 3.2, we have:

$$f(t) = m\frac{d^2x}{dt^2} + b\frac{dx}{dt} + k(x) \tag{3.3}$$

For zero initial conditions, the Laplace transform of Eq. 3.3 becomes:

$$F(s) = Ms^2X(s) + BsX(s) + KX(s) \tag{3.4}$$

The transfer function is then summarized by Eq. 3.5

$$\frac{X(s)}{F(s)} = \frac{1}{ms^2 + bs + k} \tag{3.5}$$

3.2.3 Performance measures for second-order feedback systems

We consider the transfer function of a second order feedback system, with input $r(t)$ and output $y(t)$. The transfer function for this case has the general form:

$$\boxed{G(s) = \frac{\omega_n^2}{s^2 + 2\zeta\omega_n s + \omega_n^2}; 0 < \zeta < 1} \tag{3.6}$$

where ζ is the dimensionless damping ratio and ω_n is the natural frequency (also sometimes referred to as the undamped frequency). Assuming a step input $r(t)$ is applied to this system, the solution for the output is the inverse Laplace transform of:

$$Y(s) = \frac{\omega_n^2}{s^2 + 2\zeta\omega_n s + \omega_n^2} \times \frac{1}{s}$$

$$\boxed{y(t) = \frac{1 - e^{-\zeta\omega_n t}}{\sqrt{1-\zeta^2}} \sin(\omega_d t + \Theta);\ t \geq 0} \tag{3.7}$$

where $\omega_d = \omega_n\sqrt{1-\zeta^2}$ & $\theta = \cos^{-1}(\zeta)$.

Figure 3.8 shows the standard transient responses of a second order system to a step input signal for typical ζ values.

For $0 < \zeta < 1$, the system is considered to be under-damped. It has an oscillatory behaviour and the poles of the transfer function are complex. For

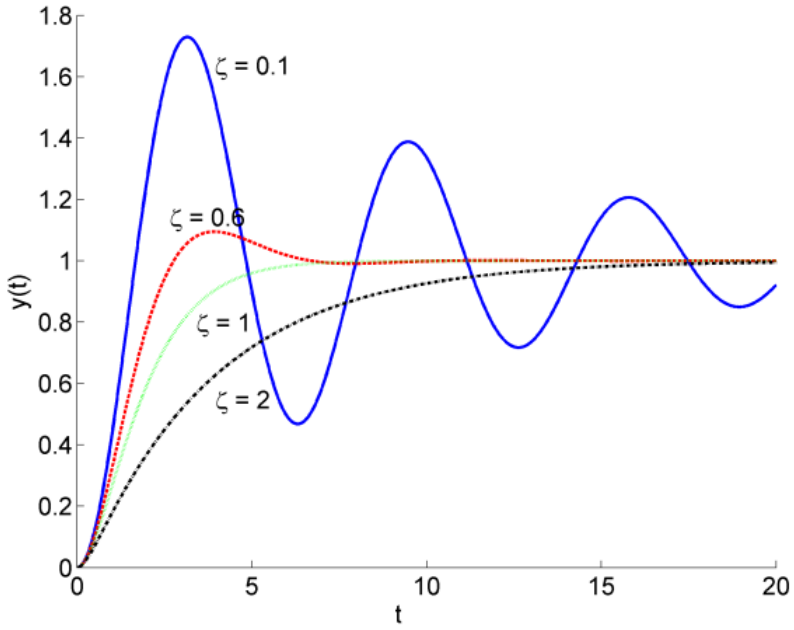

Figure 3.8: Step Response for typical ζ values

$\zeta = 1$, the system is considered to be critically damped and for $\zeta > 1$, the system is over-damped and has no oscillatory behaviour.

Figure 3.9 shows the typical form of the response of an under-damped second order system to a step input. Parameters such as **rise time**, **percentage overshoot**, **settling time** and **peak time** are used in evaluating the performance of an under-damped system with some of them represented in figure 3.9.

The **overshoot** is the maximum amount by which the response overshoots its steady state value (Bolton, 2018). It is defined by the equation:

$$\%OS = \exp^{-\left(\frac{\zeta\pi}{\sqrt{1-\zeta^2}}\right)} \times 100 \tag{3.8}$$

Solving for ζ, we have:

$$\boxed{\zeta = \frac{-\ln(\frac{\%OS}{100})}{\sqrt{\pi^2 + \ln^2(\frac{\%OS}{100})}}} \tag{3.9}$$

where

$$\%OS = \frac{y_p - y_{ss}}{y_{ss}} \times 100; \tag{3.10}$$

The **rise time**, generally represented as T_r, is the time required for the response to rise from 10% of the final value to 90% of the final value.

Settling time in simple terms is the time taken for the oscillations to die away. Dorf et al., 2000 defines it as the time required for the system to settle within a certain percentage (e.g. 2% or 5%) of the steady state value. 2% is generally the optimal settling time used for second order systems. Settling time is represented by Eq. 3.11.

$$\boxed{T_s = \frac{4}{\zeta\omega_n};\ \ for\ \zeta^2 \leq 1} \tag{3.11}$$

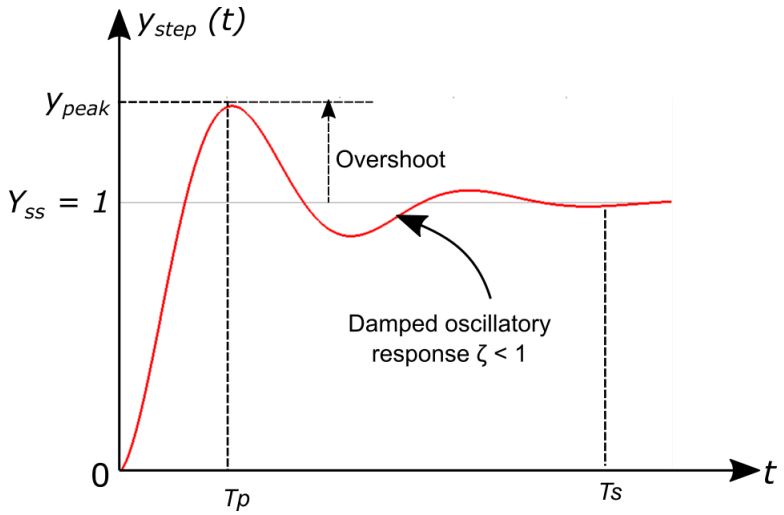

Figure 3.9: Performance characteristics of a second order system (Nise, 2011)

3.3 Laser-atom interaction and laser locking

Since we are analysing a control system to control the laser frequency for doppler cooling, it is useful as background to have a basic understanding of physics concepts such as absorption, emission and stimulated absorption. This section also gives a background on how our laser is locked using feedback control method.

3.3.1 Absorption, emission and stimulated emission

Any electron in an atom has its stable orbits called stationary states. At this point, the atom has its energy levels as illustrated by figure 3.10.

Atom radiates in terms of electromagnetic emission when an electron makes a transition from one state to the other. Bohr's principles suggests that the radia-

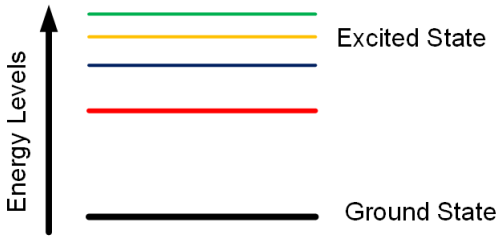

Figure 3.10: Energy levels for an electron in an atom illustrating the ground state and excited states. (Cunyun, 2004)

tion that occurs is related to the energies of the orbits and is represented by the equation:

$$v = \frac{E_f - E_i}{h} \tag{3.12}$$

where E_f and E_i are the energy levels of final and initial respective states of an atom, h is Planck's constant ($6.625 \times 10^{-34} Joul - sec$). There are three different types of electron transition that occur when an electron interacts with radiation. They are *resonant absorption*, *spontaneous emission* and *stimulated absorption*. Figure 3.11 illustrates these different transitions.

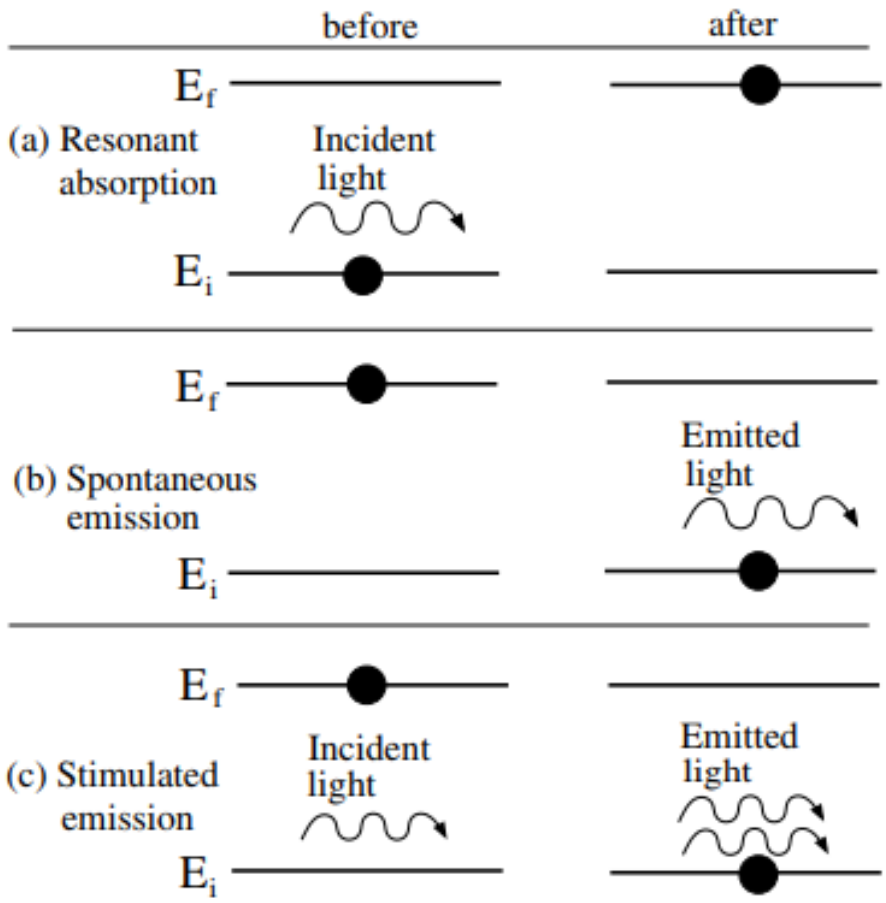

Figure 3.11: Basic frequency stabilization scheme of semiconductor diode lasers (Cunyun, 2004)

Assuming an atom is initially in a ground state E_i, the atom stays in the ground state until light with a certain frequency $v = v_0$ is applied, where v_0 is the transition between the two energy levels. In this case, there is a high probability for the atom to make a transition from a lower energy level E_i to the higher level E_f by absorption of a light quanta. This process is called the resonant absorption process as shown in figure 3.11.

After absorbing light with the atom at a higher level, this atom has a tendency to decay to a lower stable energy level. When it decays, the corresponding energy difference $E_f - E_i$ is then released by spontaneously emitting a light quantum. A photon is then emitted in a random direction with random phase. This process is defined as spontaneous emission phenomenon (figure 3.11(b)).

Fig 3.11(c) shows the third type of transition. Assuming an electron is initially in the upper state and light with frequency $v = v_0$ (i.e. $v =$ the transition frequency between two energy levels), is incident in an atom, the incident light stimulates the atom to undergo a transition from $E_f \rightarrow E_i$ in such a way that a new photon is generated. This phenomenon is known as stimulated emission. The generated light has the same phase and direction as that of the incident light and such stimulated emitted light is also known as coherent light.

Saturated absorption spectroscopy (SAS)

Basic absorption spectroscopy involves passing a laser beam through a gas sample and measuring the intensity of the beam after it passes through to get the absorption spectra of the gas of atoms. The basic arrangement for an absorption spectroscopy setup is shown in figure 3.12. By varying the frequency and measuring the intensity, we get the absorption as a function of frequency.

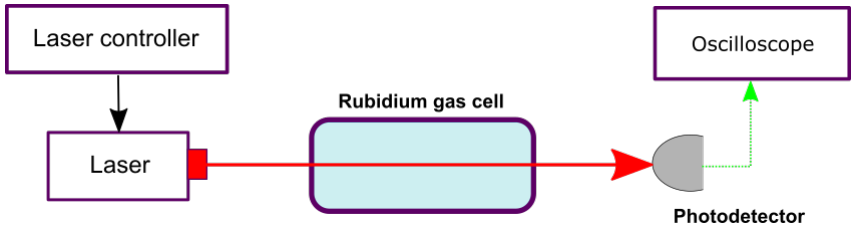

Figure 3.12: Standard absorption spectroscopy setup

However, because the atoms are in motion, they absorb the laser photons even when the atoms are not exactly in resonance with the atoms. This is due to the doppler effect. The net result is that the true spectra is now broadened due to the motion of the atom. Figure 3.13 illustrates this effect.

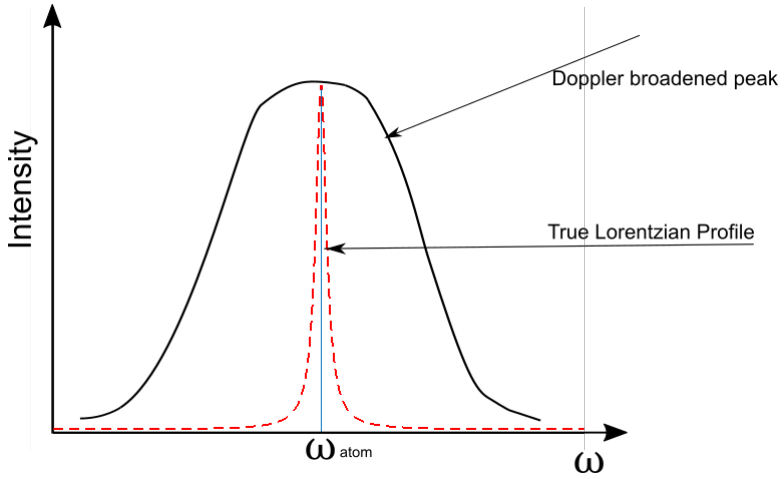

Figure 3.13: Absorption spectra using the probe beam only.

To counteract this broadening, we use a saturated absorption spectroscopy (SAS) setup, with an example of such shown in figure 3.14.

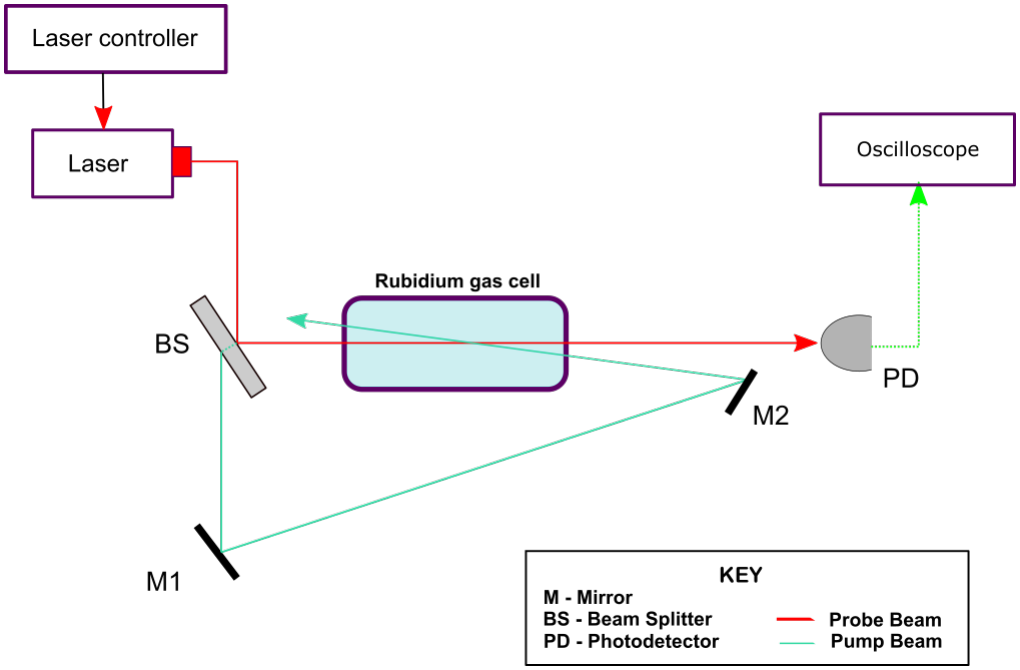

Figure 3.14: Basic saturated absorption spectroscopy setup.

It consists of a probe beam passing through the sample which we monitor using a photodetector, and a strong counter-propagating pump beam. The probe and pump beams are swept in frequency simultaneously. Because they counter-propagate, they interact with atoms of different velocities as the laser frequency is swept.

However, when the frequency is exactly in resonance (or close to resonance) with the atoms, both beams interact with the same zero-velocity atoms. The strong pump beam saturates the sample (i.e. puts the atoms in an excited state), thus leaving little atoms to interact with the probe beam, resulting in a reduction in absorption and showing its true absorption profile. This is illustrated in figure

3.15.

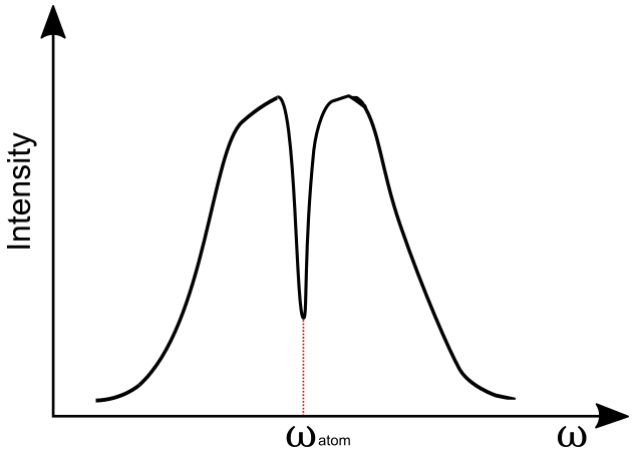

Figure 3.15: Spectra using a probe and a pump beam, showing the true absorption spectra at the resonant frequency.

It is this true absorption spectra which has a Lorentzian profile that we measure and lock on to.

3.3.2 Laser frequency locking

The overall block diagram of our feedback system to control the laser frequency is shown on figure 3.16. It consists of an external cavity diode laser which is the plant to be controlled and its power supply (laser controller), a proportional-integral-derivative (PID) controller and a feedback path.

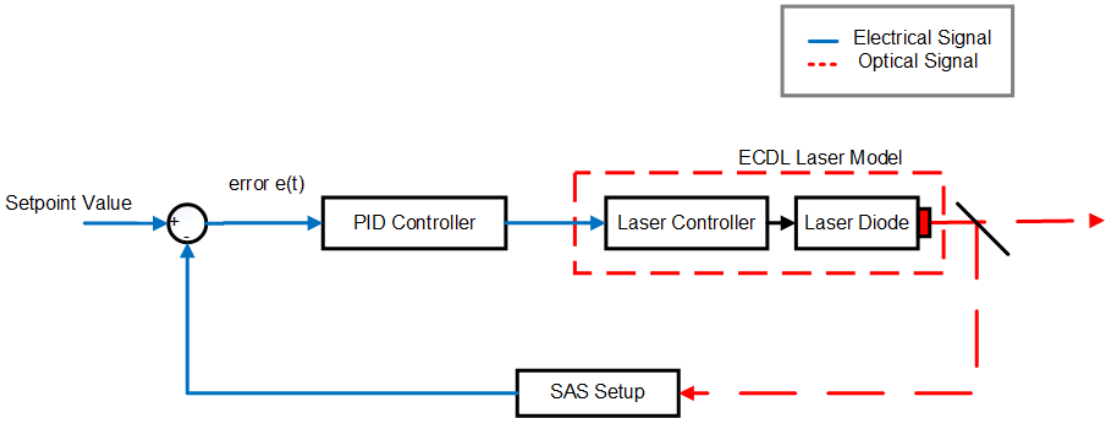

Figure 3.16: Basic frequency stabilization scheme of semiconductor diode lasers

The external cavity diode laser has been discussed in previously in chapter 1 and 2. The output laser frequency depends on various factors such as the cavity length and the diode current. The stability will depend on other factors such as vibration, temperature etc. These stability factors are difficult for the controller to predict. By using a feedback block as shown in 3.16, we can counteract the effects of these on the laser frequency as follows: The laser frequency is measured before by passing the laser beam through a setup that has frequency response we know, and the absorption of the laser is noted. This then indicates where on the absorption spectra the laser frequency is. We illustrate this concept again in figure 3.17

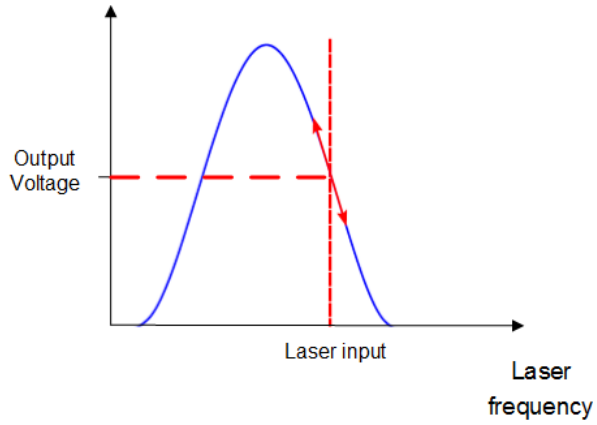

Figure 3.17: The known frequency response of the feedback block. The laser frequency is the input to the feedback element and the output is a voltage signal that is proportional to the input laser frequency

The output of the feedback network is compared to a setpoint value to create an error signal $e(t)$. This error signal is then fed to a proportional-integral-derivative (PID) controller. The P amplifies the error, then integrated and sometimes also differentiated (Bolton, 2018). The output of the PID controller is then fed to the laser. More detail on the proportional-integral-derivative (PID) controller is given below.

Proportional-Integral-Derivative (PID) Controller

The proportional-integral-derivative (PID) Controller in general has the following structure:

$$e_p = K_P e \tag{3.13}$$

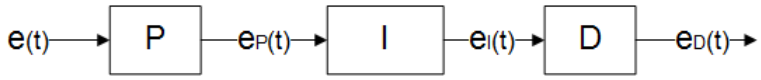

Figure 3.18: A proportional integral derivative (PID) control system

where K_P is a constant that can be adjusted.

$$e_I = K_I \int e_p dt; \tag{3.14}$$

i.e. the signal is integrated, where K_I is a constant that can be adjusted to set the integrator time constant.

and

$$D = K_D \cdot \frac{de_I}{dt} \tag{3.15}$$

where K_D is also a constant that can be adjusted.

As discussed earlier, the P block amplifies the error signal, then followed by an integrator and a differentiator. The integrator responds to slow changes in the error, while the differentiator responds to rapid changes to the system error.

The dynamical characteristics of the feedback system will depend on the choice of K_P, K_I and K_D. The table 3.2 shows how various parameters are affected with increasing values of K_P, K_I and K_D.

Table 3.2: Effect of each PID controller elements in a closed-loop control system (Tehrani et al., 2012)

Parameter	**Rise Time**	**Settling time**	**Overshoot**	**Steady-state error**
K_P	Decrease	Small change	Increase	Decrease
K_I	Decrease	Increase	Increase	Significant decrease
K_D	Small decrease	Small decrease	Small decrease	No effect (in theory)

In our actual PID controller however, the Derivative part is not used.

3.4 Summary

We have discussed the relevant theoretical concepts in context of this research. We expanded on feedback control theory and basic atomic physics concepts. We then went on to explain how a closed-loop system can be used to control the frequency of a laser beam using a PID controller and a saturated absorption spectroscopy (SAS) setup.

Chapter 4

Experimental Analysis of the Feedback Control of an External Cavity Diode Laser (ECDL)

4.1 Introduction

In this chapter, we discuss how we experimentally analysed the feedback control system used to lock the laser frequency. We describe how the existing system works, the different operating modes and how we go about locking the laser to a specific frequency.

We then discuss the results from our experiments. We first show the output

before and after the laser was locked. We also show the results from applied test input signals. The step response particularly was evaluated to observe the transient response and to extract the control parameters such as ω_n and ζ. These parameters were then used to estimate the transfer function of the system.

4.2 Overview

For easier cross-referencing, we repeat the experimental block diagram from chapter 2 in figure 4.1, but redrawn slightly differently.

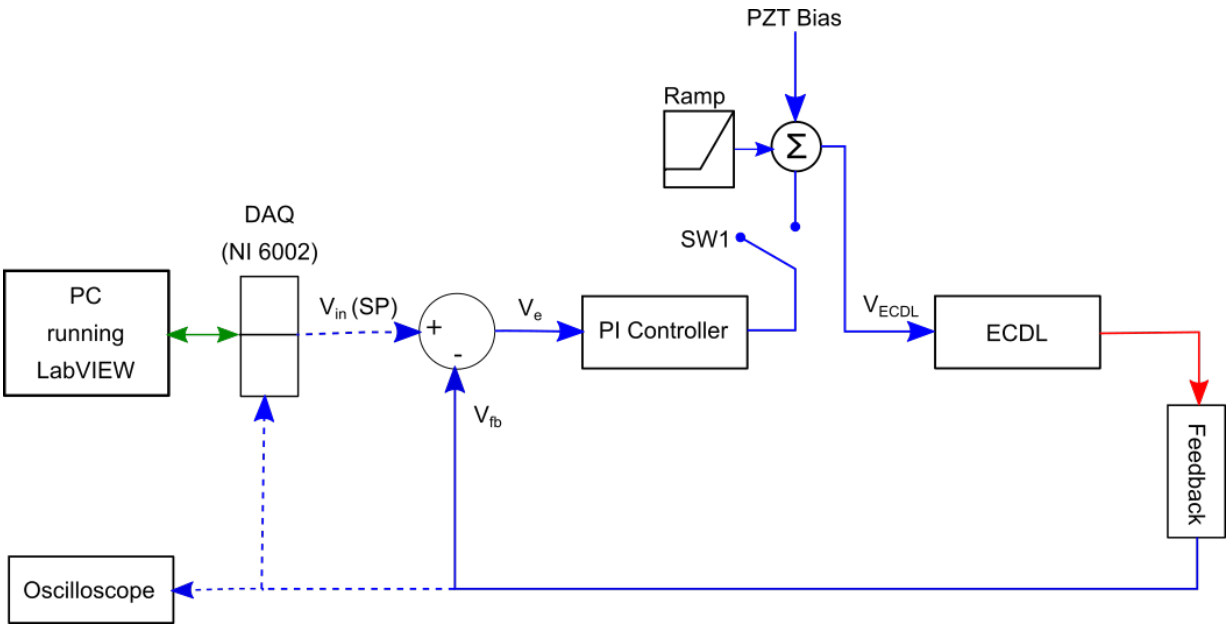

Figure 4.1: Experimental setup of the laser locking control system

The external cavity diode laser (ECDL) is the plant to be controlled, its output frequency more specifically. The signal which is applied to the external cavity diode

laser (V_{ECDL}), is a voltage which drives the piezo device in the external cavity diode laser to control the cavity length[1]. As discussed previously in chapter 2, by controlling the cavity length, we can control the frequency of the laser.

The lockswitch SW1 is used to operate the system either in open-loop mode (SW1 = open) or closed-loop mode (SW1 = closed). Open-loop operation involves the ramp and PZT bias signals as the only input sources to the laser. The ramp input is used to sweep the laser frequency over a band that is required. This function is needed initially to locate the resonant frequencies of rubidium gas of which we will lock on to. The rubidium gas mentioned is contained in a glass cell which forms part of the measurement/feedback block in figure 4.1. This function will be discussed more later on under the operation procedure. For the closed-loop operation, the lock-switch is closed and the ramp input signal is set to zero. The input signal to the laser then is solely from the PI controller's output signal and the PZT bias.

The input to the system (V_{in}) is a voltage signal set by the data acquisition device (NI 6002) and specified in LabVIEW. This input signal is then compared with the feedback signal to generate an error signal to drive the PI controller.

The signal from the feedback block (V_{fb}) is derived from a saturated absorption spectroscopy setup. The output of the feedback block is related to the absorption spectra of rubidium, since the laser is passed through a cell containing rubidium

[1]See chapter 2 for more information on external cavity diode lasers (ECDL)

gas. In open-loop control, the output has a Lorentzian profile similar to figure 4.2 for one peak. More information on the experimental setup can be found in chapter 2.

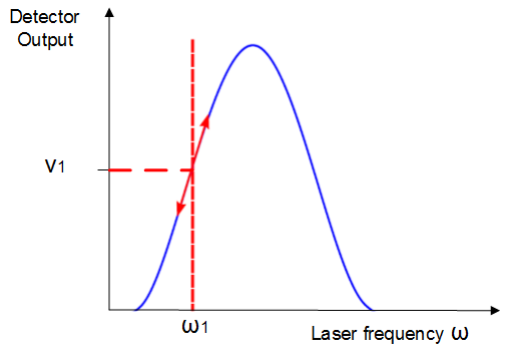

Figure 4.2: Frequency response of the feedback block (SAS setup), where the input to the system is equivalent to the output laser frequency

The feedback output is compared with the setpoint input to generate the error signal. The PI controller then operates on the error to maintain the laser at the desired setpoint frequency.

4.3 Operation modes

We experimentally perform our analysis on the control system in open-loop mode and closed-loop mode. These operation modes are discussed further below.

4.3.1 Open-loop mode

The relevant parts of figure 4.1 that are used here is shown in figure 4.3. This mode simply involves the plant (ECDL), the saturated absorption spectroscopy (SAS) setup to measure the laser frequency, the PZT bias and the ramp as the input to the ECDL. It operates with the lockswitch open and the ramp on.

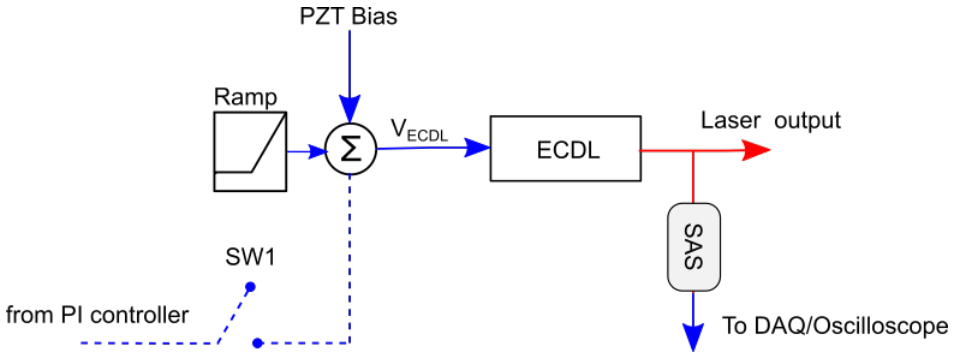

Figure 4.3: Block diagram for open loop control operation

For this mode, the SAS setup simply acts as a sensing element for the laser output. The ramp is used to sweep the frequency across a frequency band[2]. By adjusting the ramp and PZT bias input signals, we can observe the peaks of absorption of the rubidium gas. This observation is monitored either through an oscilloscope or LabVIEW[3]. The figure below shows a schematic plot of the ramp and typical absorption peaks that one may see on the oscilloscope.

[2]Recall that the input to the ECDL controls the piezo voltage, which adjusts the cavity length, which in turn varies the laser's resonant frequency.

[3]Data capturing is discussed in later section

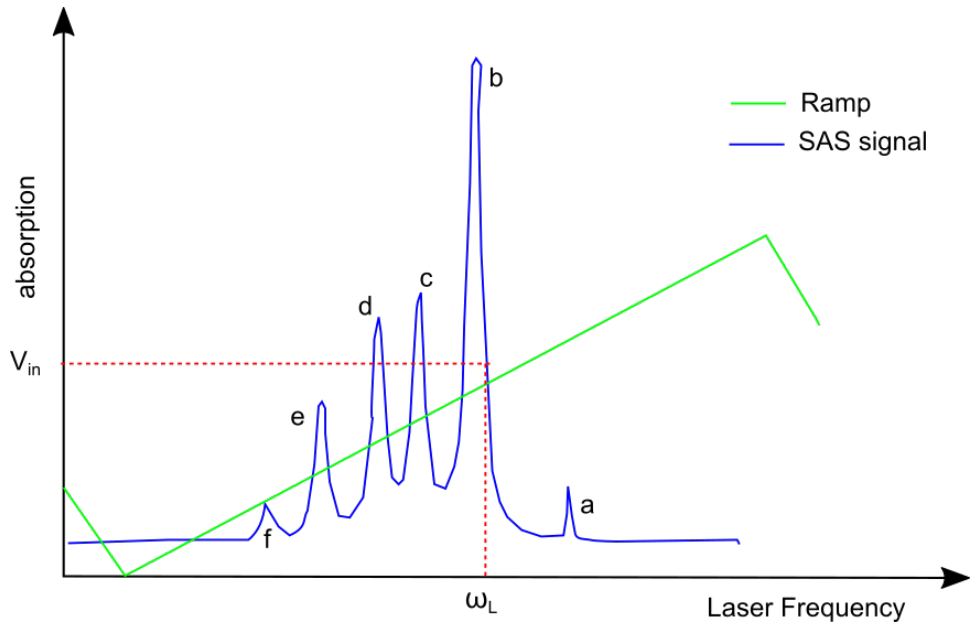

Figure 4.4: System output illustration from open-loop control mode

4.3.2 Closed-loop mode

In closed-loop mode, SW1 is closed and we want the laser output to be a selected frequency, corresponding to a value that resides towards either of the left or the right side of a chosen peak.

Let's say we want to lock the laser to a frequency ω_l as shown in figure 4.4, then the corresponding voltage V_{in} on the y-axis will be fed as an input to the closed-loop system, corresponding to the setpoint (SP) in figure 4.1. If the laser frequency drifts away from ω_l, then the PI controller will adjust the error and correct the system to achieve the desired setpoint frequency (V_{in}). The process of choosing a peak to lock on to is discussed in a later section.

While the system is locked to the side of a particular peak, we further apply sudden changes to the SP signal to see how the system responds.

Signal Injection Method

The setup to create the setpoint signal consists of a data acquisition device (NI 6002) and a PC running LabVIEW. It is used to generate input signals to the system (setpoint & test signals) and acquire data from the feedback system.

The test signals are used to carry out further performance tests on the feedback system. For more on how test signals works, see chapter 3. For our experiments, we generate step and pulse test signals. They are illustrated in figure 4.5

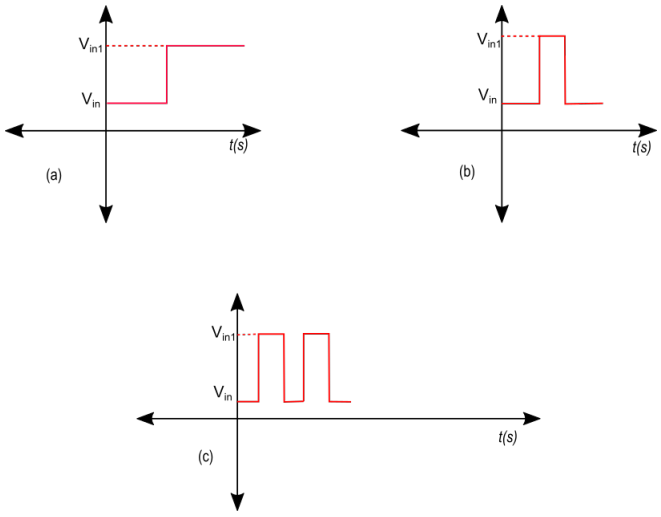

Figure 4.5: Test signals used to analyse our feedback control system. We generated a step input (a), an pulse signal (b) and multiple pulses as illustrated in (c).

4.4 Experimental procedure

In this section, we highlight the steps taken to lock the laser frequency to a specified atomic transition and how the test signals were applied to the feedback system. We start the experiment in open-loop mode. This is to observe the absorption peaks of the rubidium gas through the feedback setup. We then proceed to lock the laser frequency to a chosen frequency peak, using closed-loop operation. After the laser is successfully locked, we then carry out performance tests on the feedback system using test input signals. These tests are detailed in the next sections.

4.4.1 Open-loop control

The operation is as follows.

- The lock switch (SW1 in figure 4.1) is set to be open
- The SAS signal and ramp signal is observed on screen (either through the oscilloscope or LabVIEW)
- A ramp amplitude range is chosen to observe peaks from the SAS experiments. See figure 4.6
- The PZT bias is then adjusted to place the chosen rubidium peak at the center of the oscilloscope screen.

Figure 4.6 illustrates the output from the feedback system after the experimental steps have been taken. It illustrates the ramp and SAS output signals observed on screen.

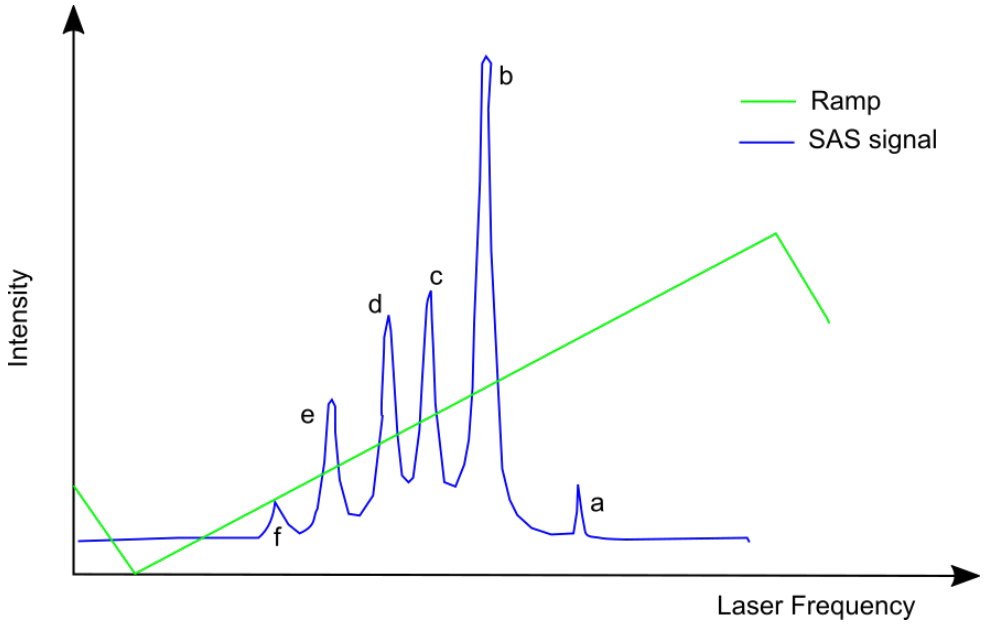

Figure 4.6: System output illustration from open-loop control mode

4.4.2 Closed-loop control

The steps taken to lock the laser are highlighted as follows. Figure 4.7 will be used as a cross-referencing tool to highlight the output from different locking stages.

- After observing the frequency output from open-loop control mode, we then identify which peak we want to lock the laser frequency to. For our experiments, we chose peak **b**.

- We adjust the setpoint voltage to the point where we want to lock the laser

frequency (see figure 4.7(b))

- We then slowly reduce the ramp while simultaneously adjusting the PZT bias to the locking point in the middle of the ramp. This process is repeated continuously until the feedback signal is reduced to an almost flat line, where the setpoint signal overlaps the feedback signal. (Figure 4.7(d)). The feedback signal becomes a flatline because the peak is magnified along the time axis as the ramp is made smaller (see figue 4.7(c) and (d))

- The lockswitch is then closed to lock the laser to the chosen setpoint.

Performance tests

After the system is observed to be locked, we apply test signals for performance analysis. We perform this operation through the following steps.

- We first configure the test signals to be applied in the developed LabVIEW program.

- We further configure the oscilloscope to capture data using a trigger. This trigger is set up such that it captures data when a sudden change in observed from the setpoint input.

- We then apply the test signal from the developed LabVIEW software.

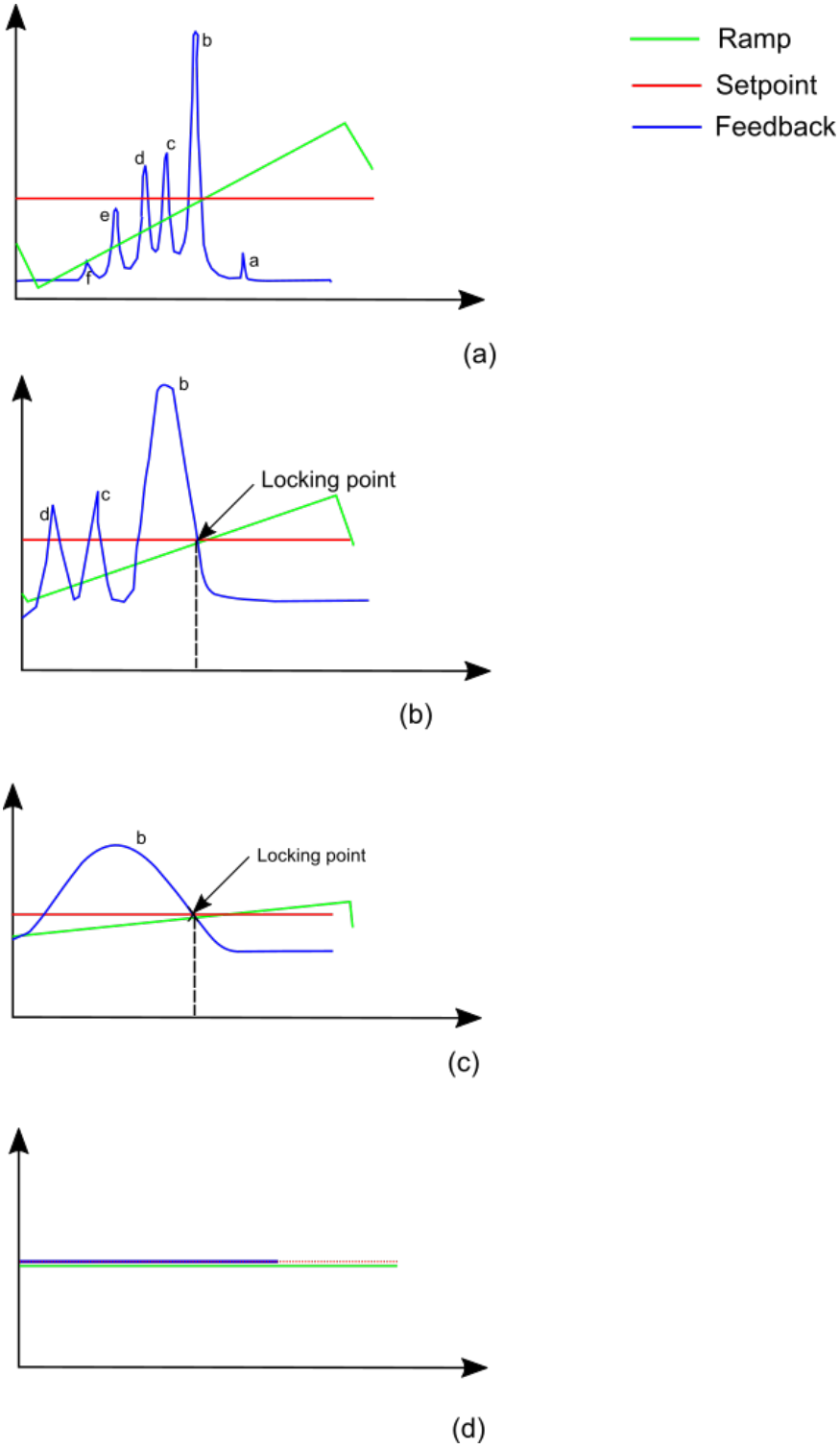

Figure 4.7: Plots illustrating the steps taken to lock the laser in closed-loop mode

4.5 Data capturing

Our data can be captured either through an oscilloscope or the data acquisition (DAQ) device (NI 6002). For basic open-loop and closed-loop operation, the DAQ is used. It is able to observe the relevant frequency band(s) from the feedback system and the locked laser signal.

For performance tests however, we use the oscilloscope alone instead. Due to the speed limits of the DAQ device, sudden changes to the system are not captured quickly enough (e.g. changes that occur in millisecond range).

4.6 Results

In this section, we show and discuss the results derived from the experiments performed as described in the previous section. These results are explained in three subsections: open-loop results, closed-loop results and parametric estimates. The results from our open-loop control tests show the absorption peaks of the rubidium gas while the results from the closed-loop tests show the laser frequency locked to a side of a chosen absorption peak[4]. We then go on to show how the system responds to different test input signals.

The applied test input signals induced a transient response on the closed-loop system. This enabled us to perform further performance tests on the closed-loop

[4]Note that this peak is identified and chosen from the open-loop tests

results. In our case, we specifically analysed the step response for the performance tests. From the step response, we were able to deduce the control parameters of the system. We then estimate the transfer function of the closed-loop feedback system using the data derived from the control parameters. We expand more on these results in the next few subsections.

4.6.1 Open-loop results

Figure 4.8 shows the results observed from our open-loop tests. These tests involve the lockswitch SW1 set as open, with the ramp and PZT Bias set as the only input sources to the laser. By adjusting the PZT Bias[5] and sweeping the ramp at a chosen frequency band, we observed the absorption peaks for a particular transition of rubidium ($^{87}R_b$) gas.

[5]The PZT Bias was simply used as an offset voltage to place the peaks at the centre of the oscilloscope screen

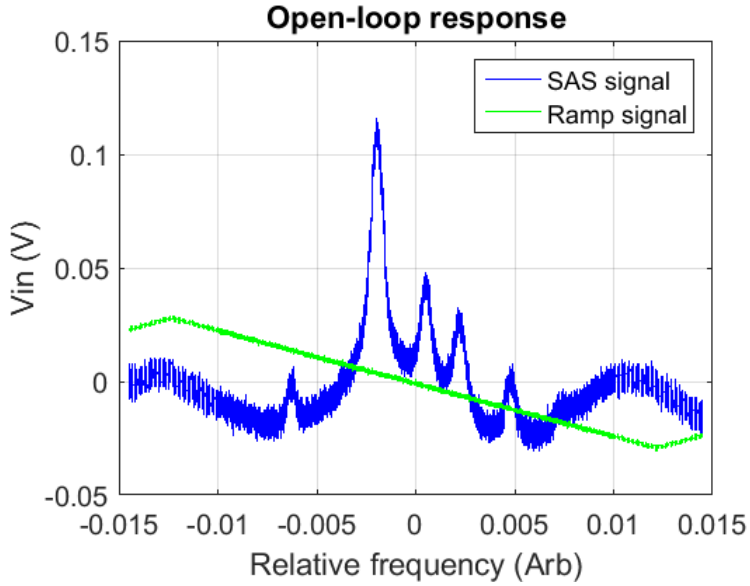

Figure 4.8: Open-loop results showing the ramp signal and the SAS signal (Hyperfine spectrum of $^{87}RbD_2(5^2S_{\frac{1}{2}})F = 2$).

As discussed earlier, the SAS signal is simply used as a sensing element for the laser output. The observed peaks acts as a reference for locking the laser, further performed in the closed-loop tests. The results from the closed-loop tests are discussed in the next section.

4.6.2 Closed-loop results

As discussed in an earlier section, the aim of the closed-loop mode is to lock the laser output to a specific value on either the left or the right side of a chosen absorption peak for performance analysis. This absorption peak is derived from the open-loop tests performed earlier as observed in figure 4.8. Also note that the

SAS signal from the open-loop results becomes the feedback signal in the closed-loop mode. The changes to this feedback signal is what we observe to monitor the laser frequency.

We first show the feedback system's transient response to different applied test signals after the lockswitch (SW1) was closed. We then proceed to analyse the parameters of the transient response to deduce it's control characteristics. From the estimated parameters, we then show the estimated transfer function of the feedback system.

System response to test signals

After we successfully locked the laser to a chosen frequency[6], we apply the test signals illustrated in figure 4.5 to the system (through V_{in} in figure 4.1). This was done to observe how the system performs to different test input signals and to induce a transient response[7]. The system response to the test input signals are shown in figures 4.9a, 4.9b and 4.9c.

[6] After closing the lockswitch SW1

[7] Remember that the transient response is required to estimate the system parameters of the feedback control system

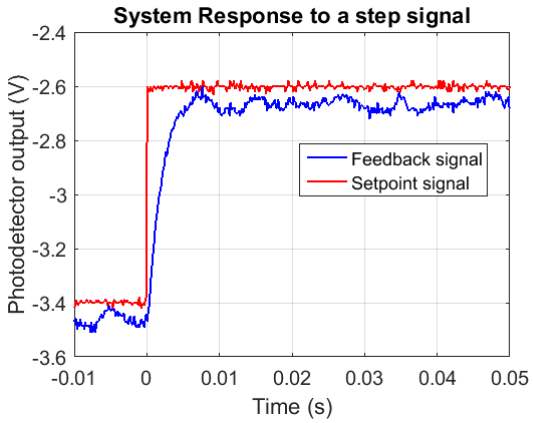

(a) The transient response of the feedback system from a step input signal

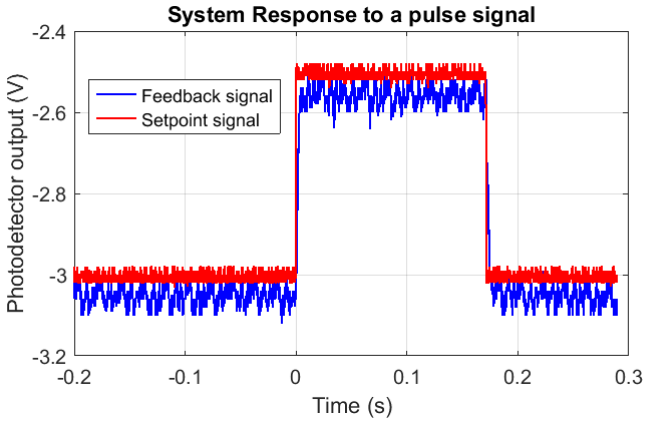

(b) The system response of the feedback system from a pulse input signal

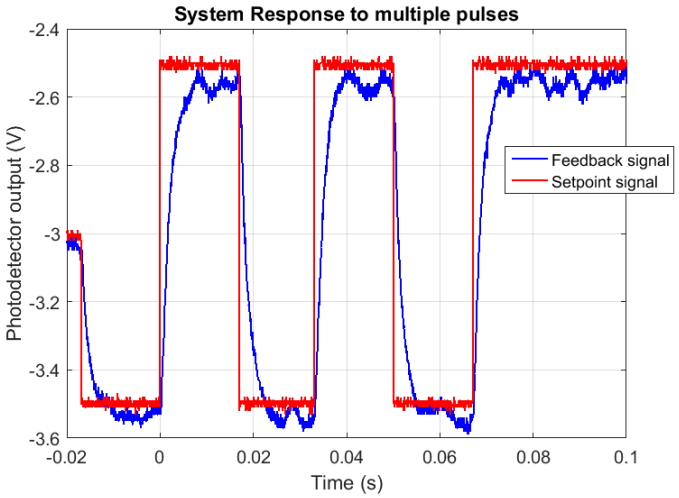

(c) System response of the feedback system to multiple pulse input signals

Figure 4.9: Results from the Closed-loop locking operation

We observe from figure 4.9 above that the system closely follows the input signal for all test scenarios. For further analysis, we focus on the results derived from the step input to analyse the feedback system. As discussed earlier, system parameters such as the damping (ζ) and resonant frequency (ω_n) can be deduced from the step response. We discuss this procedure in more detail in the next section.

4.6.3 Parameter estimatation of the closed-loop system

In this section, we estimate the transfer function of the closed-loop feedback system using data derived from the system response in the previous section. We specifically use the response derived from a step input (figure 4.9a). We first clean out the signal in Matlab using the moving average filter method[8], with the results illustrated below. Note that Y-axis was scaled to perform our analysis.

[8]see Guiñón et al., 2007 for more on this technique.

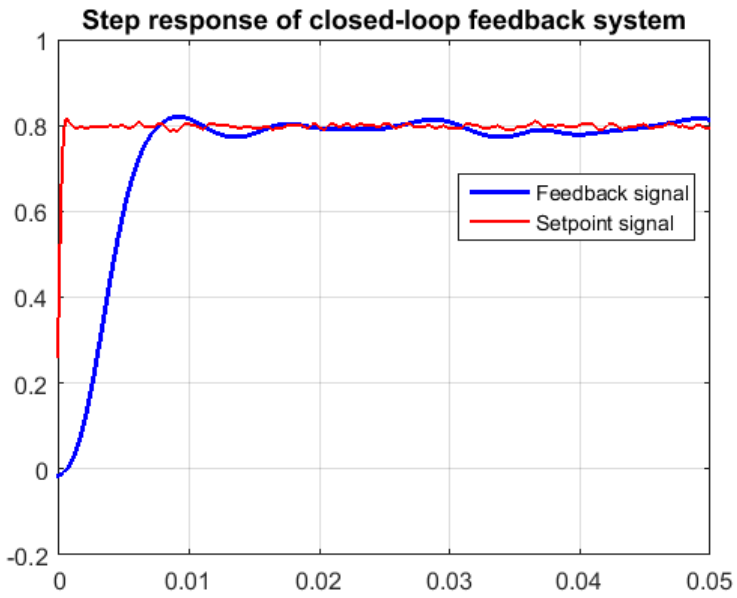

Figure 4.10: A processed step response output signal

We observe from the response in figure 4.10 that the system is slightly under-damped. To determine the transfer function of this system, we start by deducing the system parameters[9] from the system response. The feedback signal in figure 4.10 is repeated in figure 4.11 to illustrate the equivalent performance parameters discussed earlier in chapter 3. Table 4.1 shows a summary of the parameters with their estimated values.

[9]Recall from chapter 3, that the parameters are used to evaluate the performance of an under-damped system

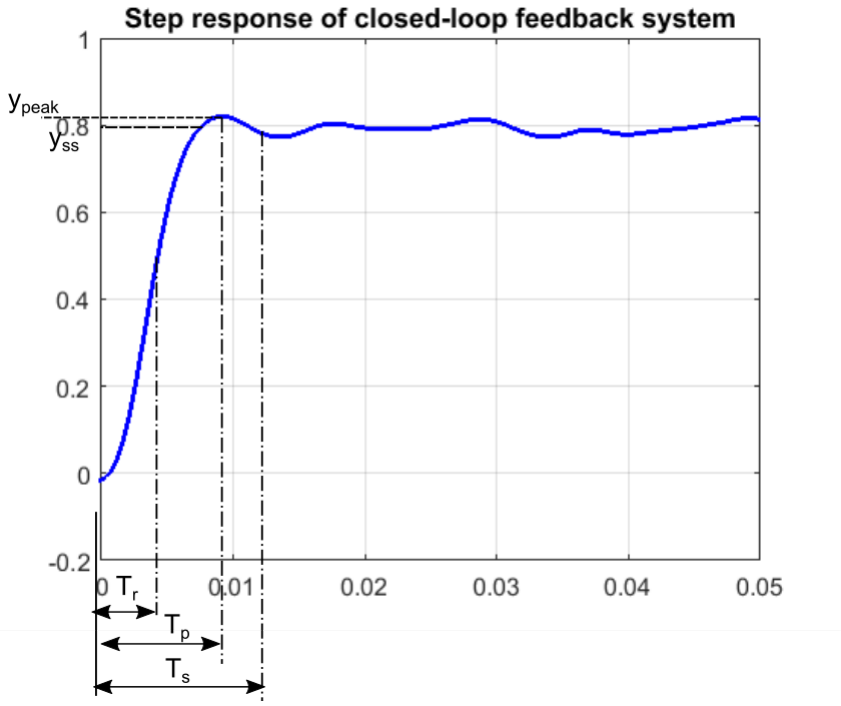

Figure 4.11: Transient response of the feedback signal to a step input, indicating the equivalent parameters

Table 4.1: Performance parameters and their estimated values

Parameters	**Value**
y_{peak}	$0.82V$
y_{ss}	$0.795V$
Peak Time T_p	$0.0085s$
Settling Time T_s	$0.012s$
Rise Time T_r	$0.007s$

Based on the values from table 4.1, we can estimate the damping constant ζ

and the resonant frequency ω_n of the feedback system. We perform this estimates using the equations discussed in chapter 3.

For a standard second order feedback system, the damping constant ζ can be estimated by the formula:

$$\zeta = \frac{-\ln(\frac{\%OS}{100})}{\sqrt{\pi^2 + \ln^2(\frac{\%OS}{100})}} \tag{4.1}$$

where $\%OS$ is the percentage overshoot. Solving for the overshoot, we have:

$$\%OS = \frac{y_{peak} - y_{ss}}{y_{ss}} \times 100 \tag{4.2}$$

$$\%OS = \frac{0.82 - 0.795}{0.795} \times 100 = 3.145 \tag{4.3}$$

$$\zeta = \frac{-\ln(\frac{3.145}{100})}{\sqrt{\pi^2 + \ln^2(\frac{3.145}{100})}} \tag{4.4}$$

Solving eq. 4.4, the damping ratio ζ becomes 0.74.

We can also solve for ω_n from eq. 4.5

$$\omega_n = \frac{4}{T_s\zeta} = \frac{4}{0.012 \times 0.74} = 450.27 rad/s; \tag{4.5}$$

We know that for a standard second order feedback system, for $0 < \zeta < 1$, the transfer function can be represented by:

$$G(s) = \frac{\omega_n^2}{s^2 + 2\zeta\omega_n s + \omega_n^2}; \tag{4.6}$$

We can then represent the transfer function of our closed-loop feedback system by:

$$G(s) = \frac{450.27^2}{s^2 + 2 \times 0.74 \times 450.27 s + 450.27^2}; \tag{4.7}$$

$$\boxed{G(s) = \frac{2.03 \times 10^5}{s^2 + 666.7s + 2.03 \times 10^5};} \tag{4.8}$$

The transfer function from eq. 4.8 was analysed in Matlab to see how it compared with our experimental results, with the results shown in figure 4.12.

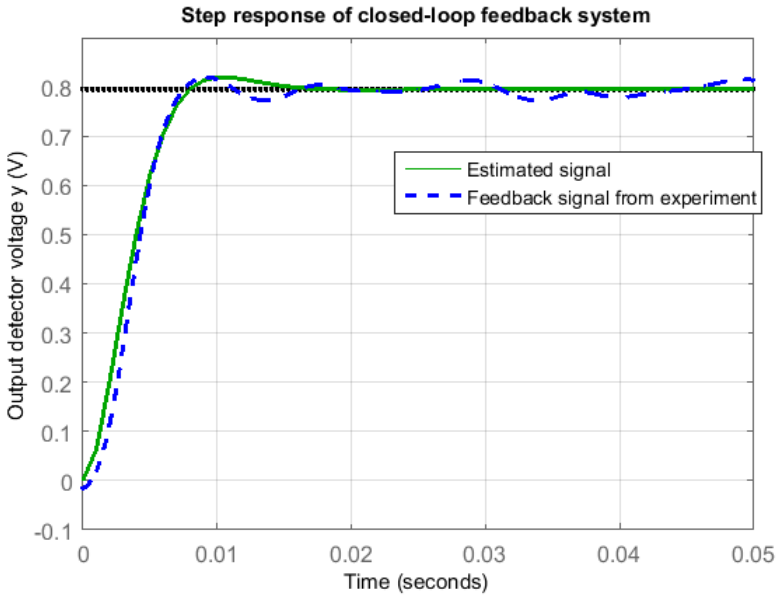

Figure 4.12: Experimental vs estimated step response

We observe the approximate similarities between experimental and estimated feedback system. They both have similar parameters such as the settling time, rise time and the peak time, thus proving our transfer function estimation to be correct.

This result will be further used later in our numerical analysis. This is discussed in the next chapter (Chapter 5).

4.7 Summary

In this chapter, we have detailed how we experimentally analysed the closed-loop system. We explained our laboratory setup and how the experiments were oper-

ated. We further went on to show how test signals were applied to the feedback system to induce a transient response.

The results obtained from the transient response was further analysed to extract the control parameters (ω_n & ζ). These parameters were then used to estimate the transfer function of the closed-loop system.

In the next chapter, we use the estimated parameters to perform a numerical analysis of the closed-loop feedback system.

Chapter 5

Numerical Analysis of the Feedback Control of an External Cavity Diode Laser (ECDL)

5.1 Introduction

In this chapter, we describe how we analysed our closed-loop feedback system numerically. We first break down the system into components, analysing and modelling them using mathematical laws and concepts. We then provide a flowchart to show how the overall closed-loop system is implemented in software.

This chapter ends with results of the simulation where we tested the closed-loop

dynamics for the following:

- determine the response for various K_p values
- effect of varying the integrator time constant
- response to a step change in setpoint
- response to an impulse change in setpoint
- response to disturbance on the cavity length
- response to disturbance applied to feedback signal

5.2 Feedback control system overview

For completeness and ease of reading, figure 5.1 shows the overview of the closed-loop feedback control model of the external cavity diode laser (ECDL) again. The closed-loop system consists of a Proportional-Integral (PI) controller, an external cavity diode laser (ECDL) and a feedback block (Stubbs, 2010).

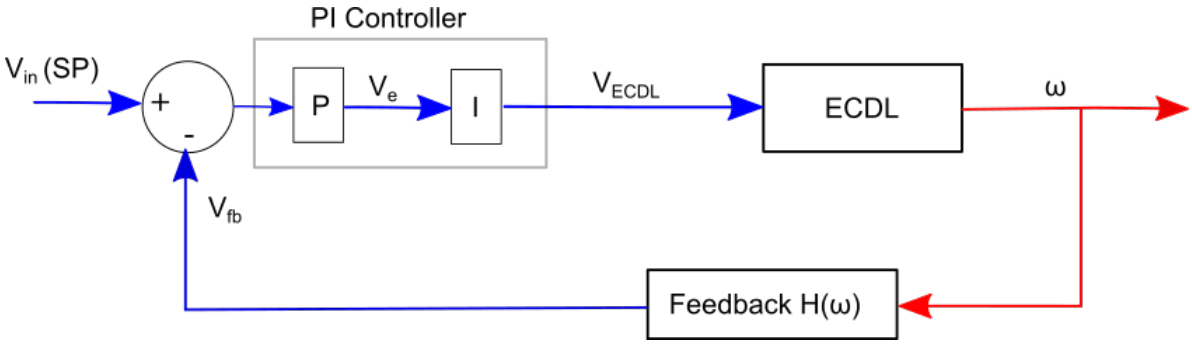

Figure 5.1: Physical layout of the ECDL closed-loop control model

The external cavity diode laser (ECDL) is the plant to be controlled. As mentioned previously, it has a piezoelectric device that behaves as a mass-spring-damper system and its change in length (deflection) determines the change in output frequency. The laser frequency is optimized by varying the proportional (P) and integral (I) coefficients. The feedback block measures the frequency from the plant (ECDL) and produces an output voltage which is proportional to the frequency. This is then compared with the initial setpoint frequency/voltage to get the error signal. This error signal is fed into the Proportional-Integral controller (PI) unit. This unit amplifies the signal with a P coefficient and integrates it. This forms a control signal that is then sent to the plant to adjust the response to desired frequency.

Below we give a detailed description of the composition of each block and equations used to implement the numerical simulation of each block.

5.2.1 External cavity diode laser (ECDL) model

The detailed construction of the external cavity diode laser has been described in a previous chapter (chapter 2). From that discussion, we know the external cavity diode laser has a piezoelectric device that behaves as a mass-spring-damper system. When a force u is applied to the piezoelectric crystal, its atoms are displaced slightly from their initial positions, thus creating a change in the thickness of the piezoelectric device, which in turn changes the cavity length (Bentley, 1995). The frequency of the cavity resonance is given by the equation:

$$\boxed{\omega = 2\pi \frac{cn}{L_0 + y}} \tag{5.1}$$

where L_0 is a constant, y is the change in piezo thickness, c is the speed of light and n is an integer.

The force in this case will be an input voltage V_{ECDL}, an output signal from the PID controller[1]. The relationship between the displacement y and the input force V_{ECDL} is represented by transfer function:

$$\frac{Y(s)}{V_{ECDL}(s)} = \frac{\dfrac{1}{k}}{\dfrac{1}{\omega_n^2}s^2 + \dfrac{2\zeta}{\omega_n}s + 1} \tag{5.2}$$

where ω_n is the resonant frequency, k is the stiffness of the crystal, ζ is the damping

[1]This will be discussed in more detail later in this chapter.

ratio (Bentley, 1995).

Rewriting this as a differential equation, we have:

$$\ddot{y}(t) + 2\zeta\omega_n\dot{y}(t) + \omega_n^2 y(t) = \frac{\omega_n^2}{k} V_{ECDL}(t) \tag{5.3}$$

We can represent the above 2nd order equation as two first order differential equations as follows:

Let $y_1 = y$, then

$$y_2 = \dot{y_1} = \dot{y} \tag{5.4}$$

$$\dot{y_2} = \frac{\omega_n^2}{k} V_{ECDL}(t) - 2\zeta\omega_n y_2 - \omega_n^2 y_1; \tag{5.5}$$

To determine the value of y_1 for various sampled time instances, we implement the above equation numerically using the Euler method as follows:

$$\boxed{y_1(n) = \Delta t * y_2(n-1) + y_1(n-1);} \tag{5.6}$$

$$\boxed{y_2(n) = \Delta t * (\frac{\omega_n^2}{k} V_{ECDL}(n-1) - 2\zeta\omega_n y_2(n-1) - \omega_n^2 y_1(n-1)) + y_2(n-1);} \tag{5.7}$$

where Δt is a chosen time length. We then solve for the laser frequency ω using eq. 5.1. Equations (5.6), (5.7) and (5.1) are used in the numerical model of the ECDL in the simulation.

5.2.2 Feedback block model

As discussed in chapter 2, we measure the laser frequency using saturated absorption spectroscopy (SAS). This involves passing the laser light through a reference gas whose frequency response (absorption as a function of frequency) is known. The reference gas used in our case is rubidium (^{85}Rb and ^{87}Rb). Figure 5.2 shows the hyperfine spectra of ^{87}Rb from a saturated absorption spectroscopy experiment[2], with the FWHM of each peak in the MHz range.

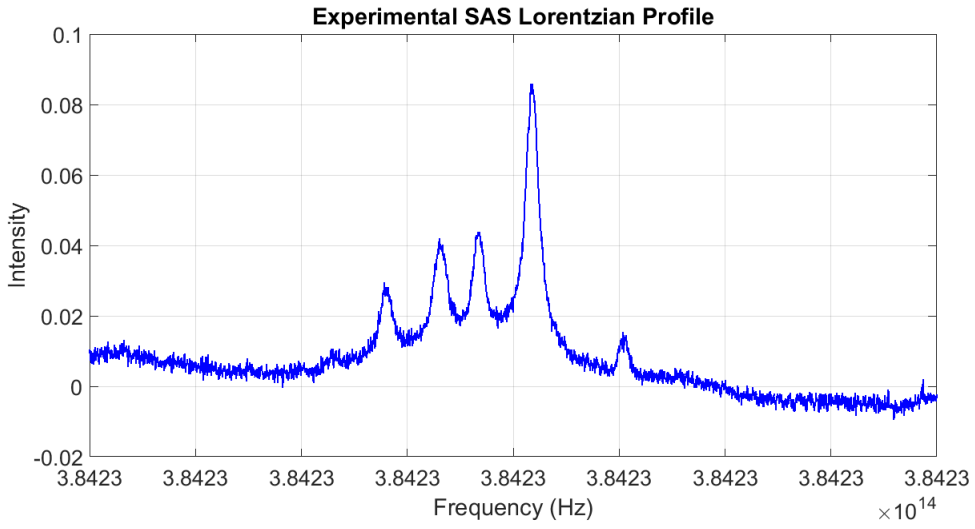

Figure 5.2: Hyperfine Spectrum of $^{87}Rb, F = 2toF_1 = 1, 2, 3$

[2]Experimental Study of the Weak Field Zeeman Spectra of ^{85}Rb and ^{87}Rb

For simulation purposes however, we use an arbitrary frequency scale. The absorption profile of the rubidium gas sample is defined by a series of Lorentzian curves. The total frequency response of the SAS is then given by:

$$H(\omega) = \sum_i \frac{\Gamma^2}{(\omega - \omega_{0i})^2 + \Gamma^2} \tag{5.8}$$

where Γ is parameter that specifies the width of each curve, ω_0 is the resonant atomic transition frequency of the i^{th} peak and ω is the laser frequency. Figure 5.3 shows a matlab plot of the absorption profile where each peak has been modelled using a Lorentzian profile with spectra values for Γ and ω_0.

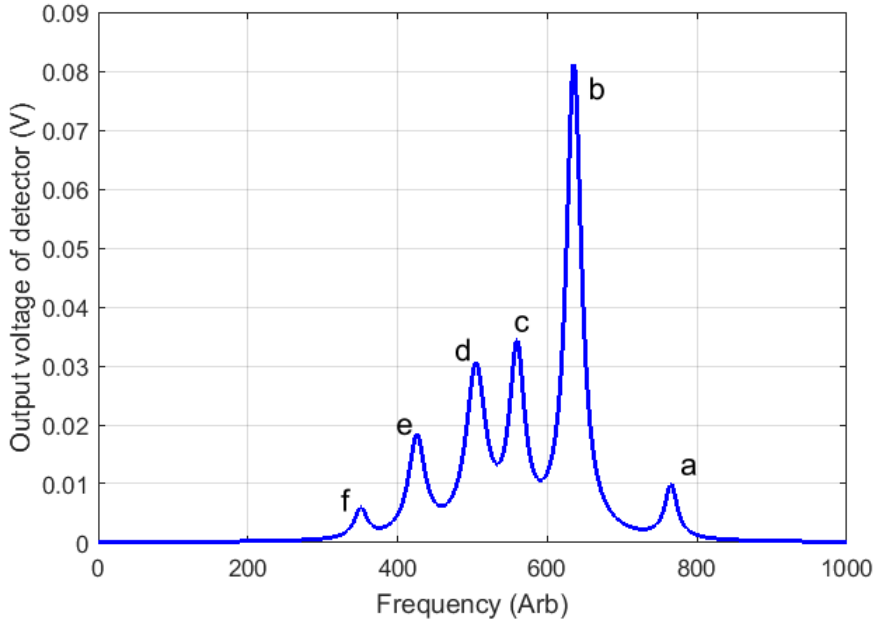

Figure 5.3: Simulated equivalent of the Hyperfine spectrum of $^{87}Rb, F = 2 to F_1 = 1, 2, 3$

Note that to derive the value of Γ, we plot the curve such that it overlapped the experimental data and varied Γ so that the plots matched each other. We plot the function with different values (through trial-by-error) until the simulated curves matched the experiment. The output of the feedback block (V_{fb}) is then determined by substituting the value ω (calculated in eq. 5.1) for the laser frequency to eq. 5.8. It is this value that is compared with the setpoint input (V_{sp}) to get the error $e(t)$ (V_e in figure 5.1), which is then fed into the proportional-integral (PI) controller unit. Note that we are using an arbitrary frequency scale for simulation purposes.

5.2.3 Proportional Integral (PI) Controller

The P block scales the error signal between setpoint and the measured laser frequency ($V_e = K_p(V_{in} - V_{fb})$). In terms of sampled signals,

$$\boxed{V_e(n) = K_p(V_{in}(n) - V_{fb}(n))} \tag{5.9}$$

The output of the P block is then fed into the integrator.

We model the integrator by approximating it using a model of the RC circuit. Consider the following RC circuit in figure 5.4

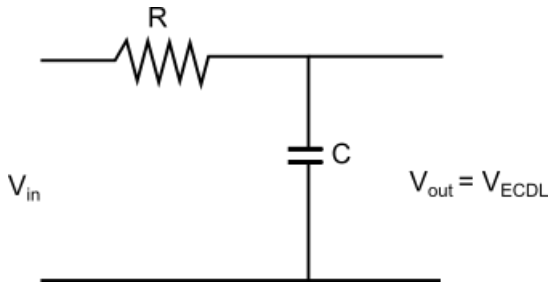

Figure 5.4: A RC circuit

Using Kirchhoffs voltage law,

$$V_{in} = V_R + V_C \tag{5.10}$$

$$V_{in} = RC\frac{dV_c}{dt} + V_C \tag{5.11}$$

Discretizing the above differential using a sampling time ΔT gives:

$$V_{in}(n\Delta T) = RC\frac{V_C(n\Delta T) - V_C(n-1)\Delta T}{\Delta T} + V_C(n\Delta T) \tag{5.12}$$

which can be written as

$$V_{in}(n) = \frac{RC}{\Delta T}\left[V_C(n) - V_C(n-1)\right] + V_C(n)$$

$$\frac{\Delta T}{RC}V_{in}(n) = V_C(n) + \frac{\Delta T}{RC}V_c(n) - V_C(n-1)$$

$$\left[1+\frac{\Delta T}{RC}\right]V_C(n)=\left[\frac{\Delta T}{RC}V_{in}(n)+V_C(n-1)\right]$$

where $V_{in}(n)$ and $V_C(n)$ are samples of $V_{in}(t)$ and $V_C(t)$.

$$V_C(n)=\left[\frac{RC}{RC+\Delta T}\right]\left[\frac{\Delta T}{RC}V_{in}(n)+V_C(n-1)\right]$$

$$V_C(n)=\left[\frac{\Delta T}{RC+\Delta T}\right]V_{in}(n)+\left[\frac{RC}{RC+\Delta T}\right]V_C(n-1) \tag{5.13}$$

$$V_C(n)=aV_{in}(n)+bV_C(n-1) \tag{5.14}$$

where

$$a=\frac{\Delta T}{RC+\Delta T},\ b=\frac{RC}{RC+\Delta T} \tag{5.15}$$

and

$$a+b=1 \tag{5.16}$$

Thus the difference equation used to implement the "integrator" in terms of variables used in figure 5.5 is given by:

$$\boxed{V_{ECDL}(n)=aV_e(n)+bV_{ECDL}(n)} \tag{5.17}$$

We choose a and b such that $a+b = 1$ and by varying a and b, we can control the integration time constant. From eq. 5.15, the integration time constant ($\tau = RC$) is:

$$a = \frac{\Delta T}{\tau + \Delta T} \tag{5.18}$$

$$\therefore \tau = \frac{1-a}{a}\Delta T \tag{5.19}$$

5.3 Software Design

Figure 5.5 illustrates the closed-loop system for our numerical simulation. Each block illustrates how each subsystem was modelled mathematically and how they are interlinked with each other.

The feedback system was simulated in Matlab. The flow diagram of our simulation is shown in figure 5.6.

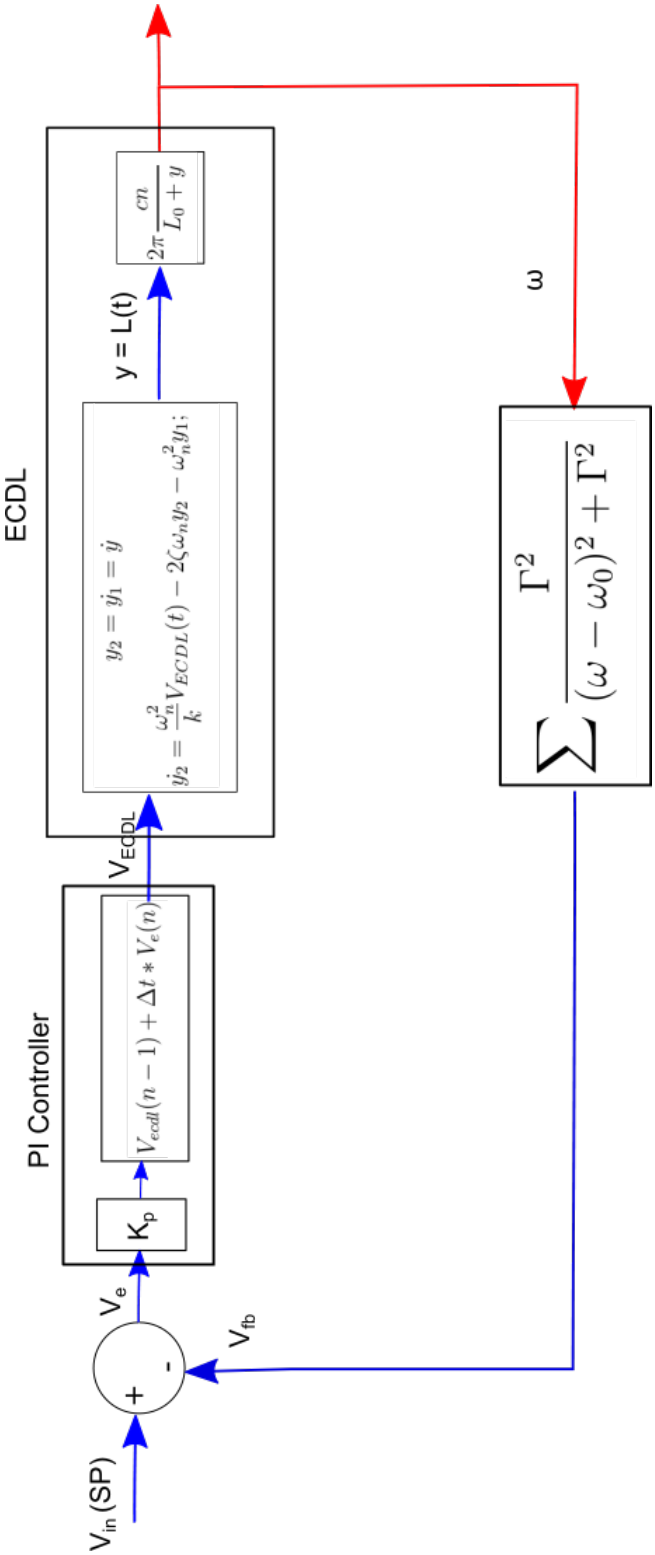

Figure 5.5: Mathematical model of the closed-loop ECDL feedback system

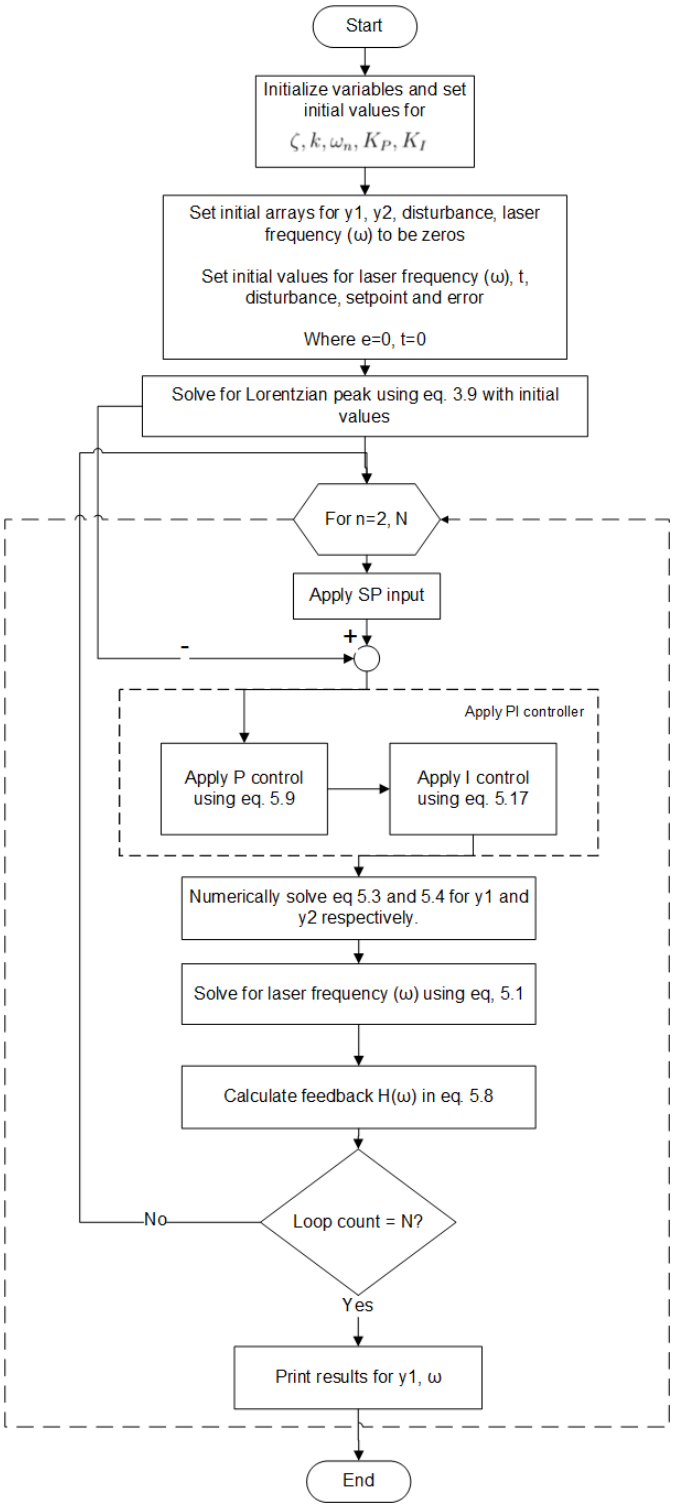

Figure 5.6: Software flow diagram

5.4 Computational results and discussion

In this section, we discuss the results measured from various performance tests applied to the numerical simulation using ω_n and ζ values obtained from the previous chapter. It is important to note that a full Laplace domain analysis and study of the closed-loop system is quite complicated and results in a 6^{th} order transfer function. However from the results in the actual experiments, the system is dominated by a second order system function. To simplify matters further for the present analysis, the ω_n and ζ found previously will be used as the natural frequency and damping constant of the laser.

We first show the system response of the feedback system to a step input. We then show how the system performs to different controller constants (i.e. various K_p & τ values). From the results observed, we proceed to optimize the controller parameters such that the settling time is similar to that of the experiments performed in the chapter 4.

We then discuss the results observed when the system is subjected to certain disturbances at different points in the feedback loop. Note that the input to the closed-loop system is in terms of voltages, which are proportional to the laser frequency. This is the input-output relationship of the feedback block (saturated absorption setup), and is in the form of a Lorentzian function.

For the tests conducted here on, we lock on the right side of the Lorentzian peak

labelled **a** in figure 5.3. For simplicity, we use '*Arb*' as the unit of measurement for the laser output frequency. It represents an arbitrary frequency unit.

5.4.1 System response to step input

Before running the simulations, we initially assume the gain (K_p) and integration constant (τ) to be 0.5 and 0.0009 respectively. Also recall that the ω_n and ζ used in our simulations were derived from the experimental analysis and they are 450.27 rad/s and 0.74 respectively.

We assume the laser is running at an undisturbed frequency of 630 *Arb*, corresponding to a setpoint (V_{in}) of 0.007 V. The response to a step change in input from $V_{in} = 0.007\ V$ to $V_{in} = 0.005\ V$ (corresponding to 632.6 *Arb*) is shown in figure 5.7.

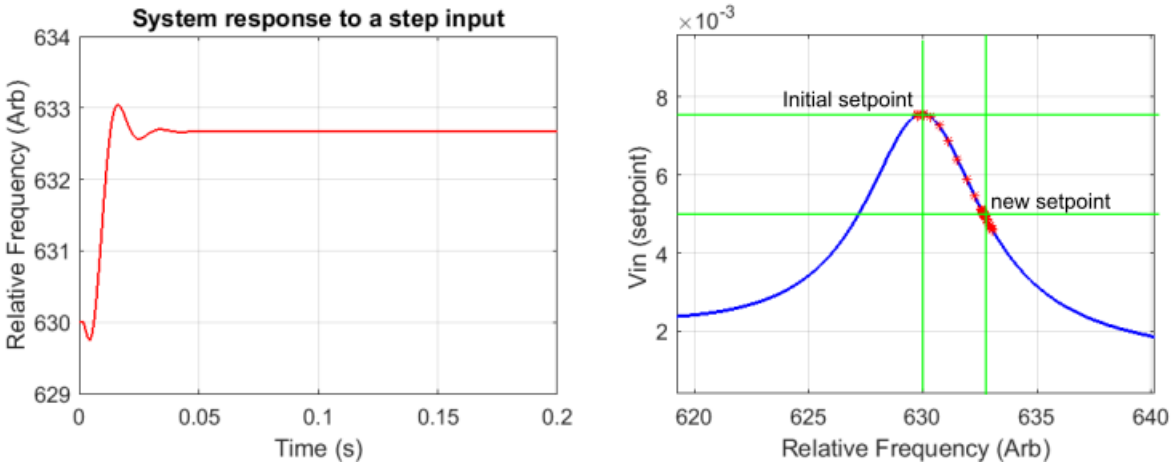

Figure 5.7: The system response to a step change $V_{in} = 0.005\ V$ to $V_{in} = 0.007\ V$. The figure on the left shows the laser frequency vs time and (b) shows how the ECDL frequency varies at the chosen peaks

We observe an underdamped transient response as the system locks to the specified setpoint. As seen in figure above, the system starts at the initial specified frequency (630 Arb), and then oscillates about the new setpoint frequency with an estimated overshoot of 0.06 %, before eventually settling down to the specified setpoint frequency (632 Arb) after 0.03 s.

5.4.2 System response to various gain (K_p) values

We simulate the system for different proportional constants (K_p). This is to investigate how the proportional controller influences the feedback system. The system was simulated for six different parameter variations i.e. $K_p = 0.2$, 0.4, 0.6, 0.8, 1 and 1.2. Using the same step change in input from $V_{in} = 0.007\ V$ to $V_{in} = 0.005\ V$, we evaluated the response of the laser frequency to the step change.

The results are shown in figure 5.8 and summarised in table 5.1.

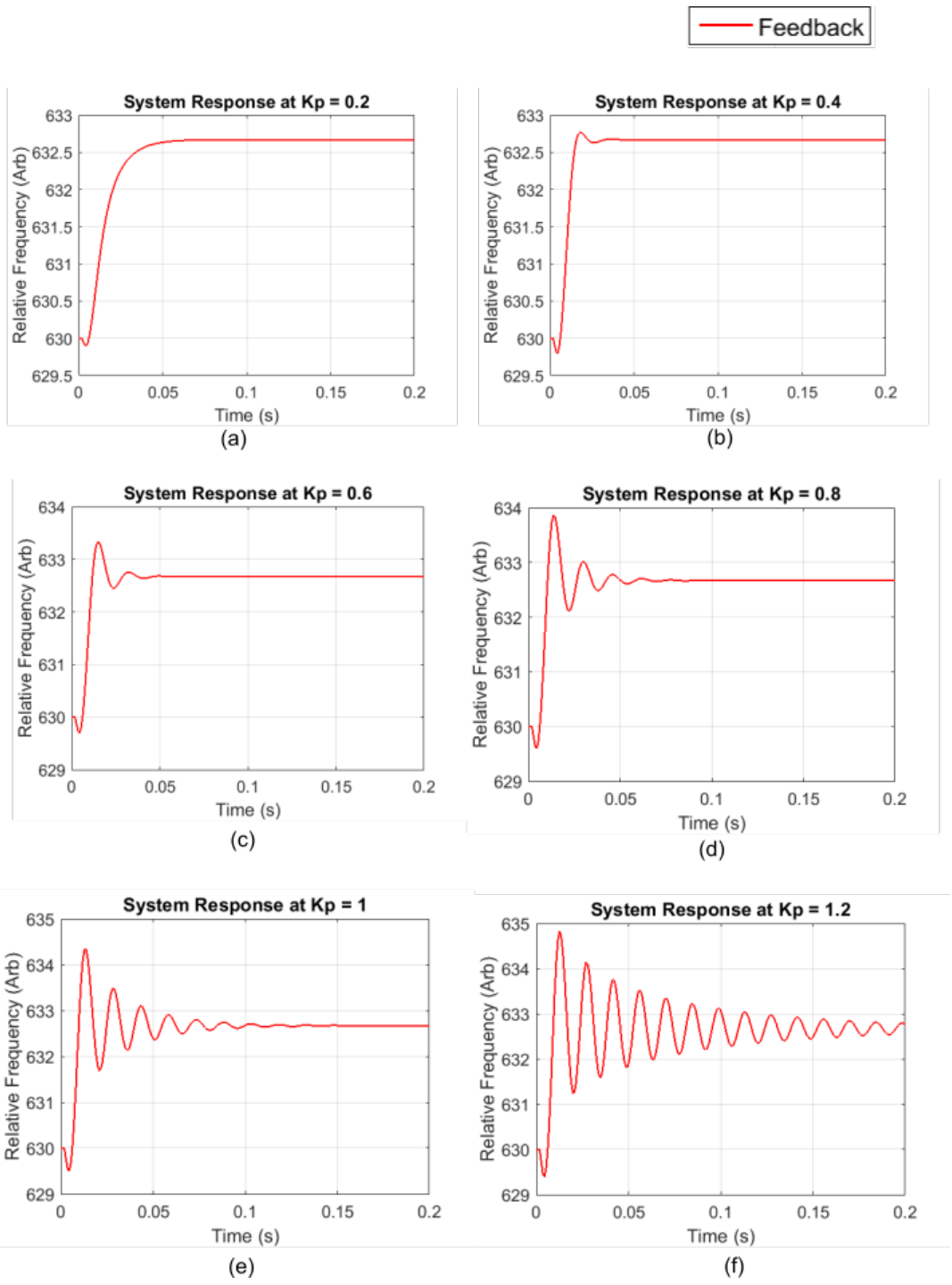

Figure 5.8: System response (laser frequency vs time) for various K_p values, and for a step change in input $V_{in} = 0.007\ V$ (630 Arb) to $V_{in} = 0.005\ V$ (632.6 Arb)

Table 5.1: Table showing performance characteristics of the closed-loop system for different proportional constants (K_p)

Plot	**a**	**b**	**c**	**d**	**e**	**f**
Kp	0.2	0.4	0.6	0.8	1.0	1.2
Ts (ms)	66	37	46	78	0.14	-
Overshoot (%)	0	1.46	1.55	1.64	1.72	1.79

We observe from figure 5.8 that the lower the gain, the slower the system's settling time. This is seen in figure 5.8(a) where the gain was set to 0.1. As the gain increases, we observe increased oscillations and overshoot in the system. As K_p goes higher, the system becomes more and more unstable.

The system performed best when the gain constant was set to 0.4 (figure 5.8(b)). The overshoot was minimal compared to the other values of K_p and the system settled the fastest at this value.

5.4.3 System response to different integrator time constants (τ)

We also test the system to observe how the integrator performs for different time constant values τ. We simulate for six cases which are summarised in table 5.2. In this case, we simulate the system by varying a and b from eq. 5.17 such that:

$$a + b = 1;$$

The different responses observed are shown in figure **??** and the results summarised in table 5.2.

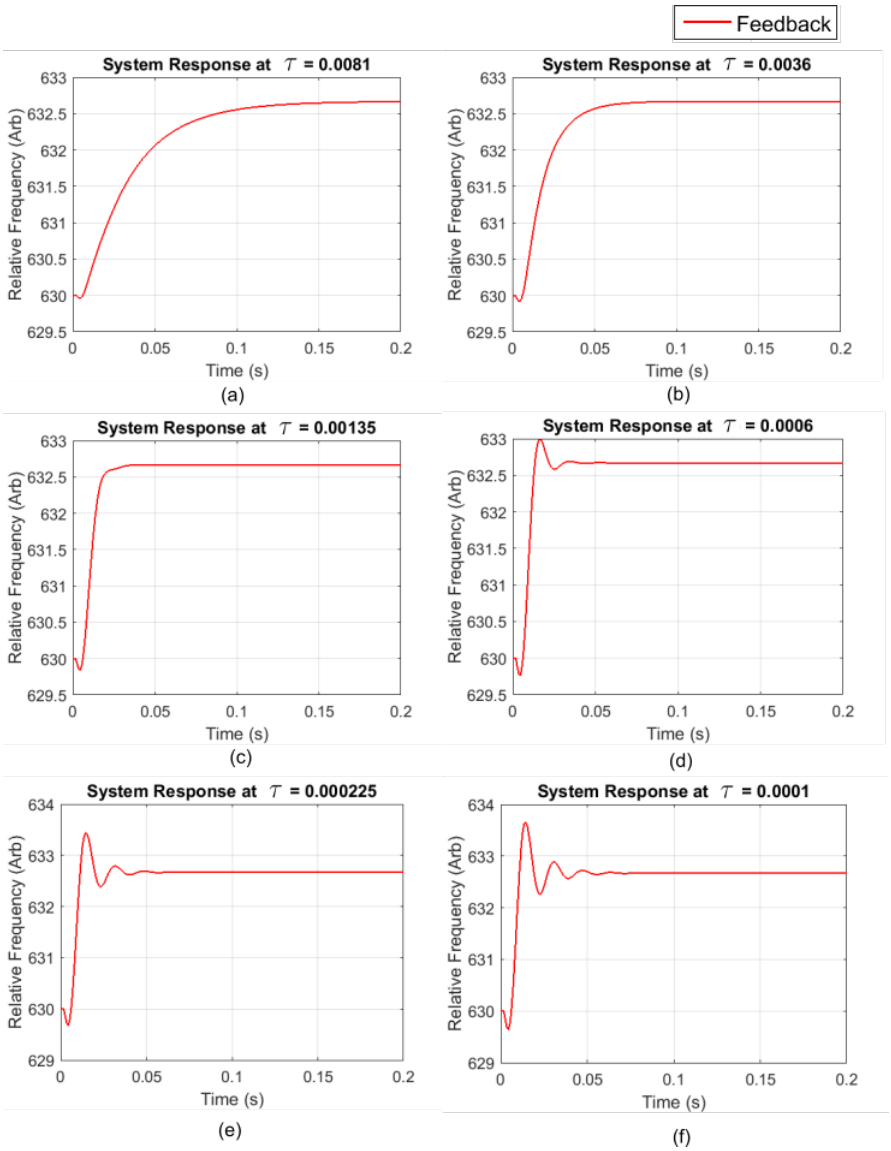

Figure 5.9: System response (laser frequency vs time) for various τ values, and for a step change in input $V_{in} = 0.005\ V$ (630 Arb) to $V_{in} = 0.007\ V$ (632.6 Arb)

Table 5.2: Table showing performance characteristics of the closed-loop system for different integration time constants (τ)

Plot	**Ki**		**Time constant τ (s)**	**Settling Time T_s (s)**	**Overshoot (%)**
	a	**b**			
a	0.1	0.9	0.0081	0.18	-
b	0.2	0.8	0.0036	0.007	-
c	0.4	0.6	0.0014	0.04	-
d	0.6	0.4	0.0006	0.041	1.50
e	0.8	0.2	0.00023	0.05	1.56
f	0.9	0.1	0.0001	0.08	1.60

From the results, we observe how the changes to the integration constants influences the feedback system. We observe that as the integration time (τ) decreases, the settling time also decreases. The overshoot however increases as τ decreases. The best result was observed at plot **d**, where $\tau = 0.0006$. At this point, the settling time is 41 ms and the overshoot is 1.5 %.

5.4.4 System response to disturbance

After optimizing the system by choosing the best K_p and τ values, we then analysed the system by applying different disturbance types to the closed-loop system. The K_p and τ values used are 0.35 and 0.0009 respectively. The disturbance points are

shown in figure 5.10. It shows the feedback system with three disturbance inputs added at various points in the system.

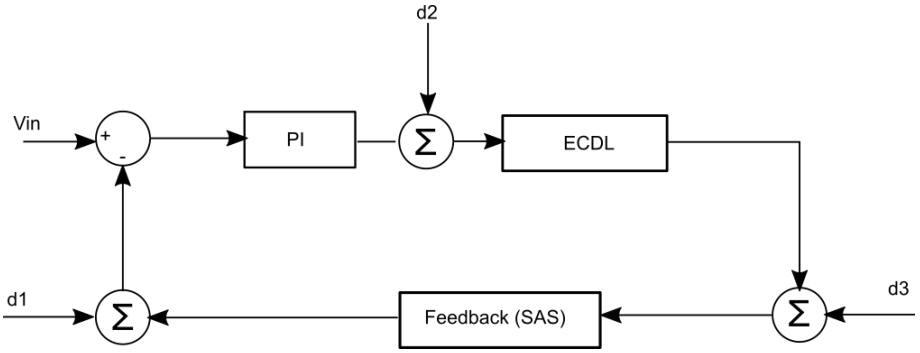

Figure 5.10: Closed-loop system showing disturbance points

The first disturbance input (**d1**) is an input added to the feedback output, **d2** is added the ECDL's input and **d3** added to the ECDL's output. We simulate the system to check for a impulse disturbance and an impulse disturbance at $t = 0.3$ s. The results observed are discussed in the next subsections.

System response to impulse disturbance

Figures 5.11, 5.12 and 5.13 show the results observed from applying an impulse disturbance to the disturbance points mentioned above, for a positive and negative magnitude of 0.1. Note that the plots on the left indicate the transient response of the closed-loop system (laser frequency vs time) while the plots on the right shows how the laser frequency moves along the chosen Lorentzian peak. Before the application of the disturbance, the laser frequency is 632.6 *Arb*. The plots on the left show the position of the applied disturbance (in black dashed line) relative

to the system output. Note that the black trace is not drawn to scale and is simply inserted to show time of application.

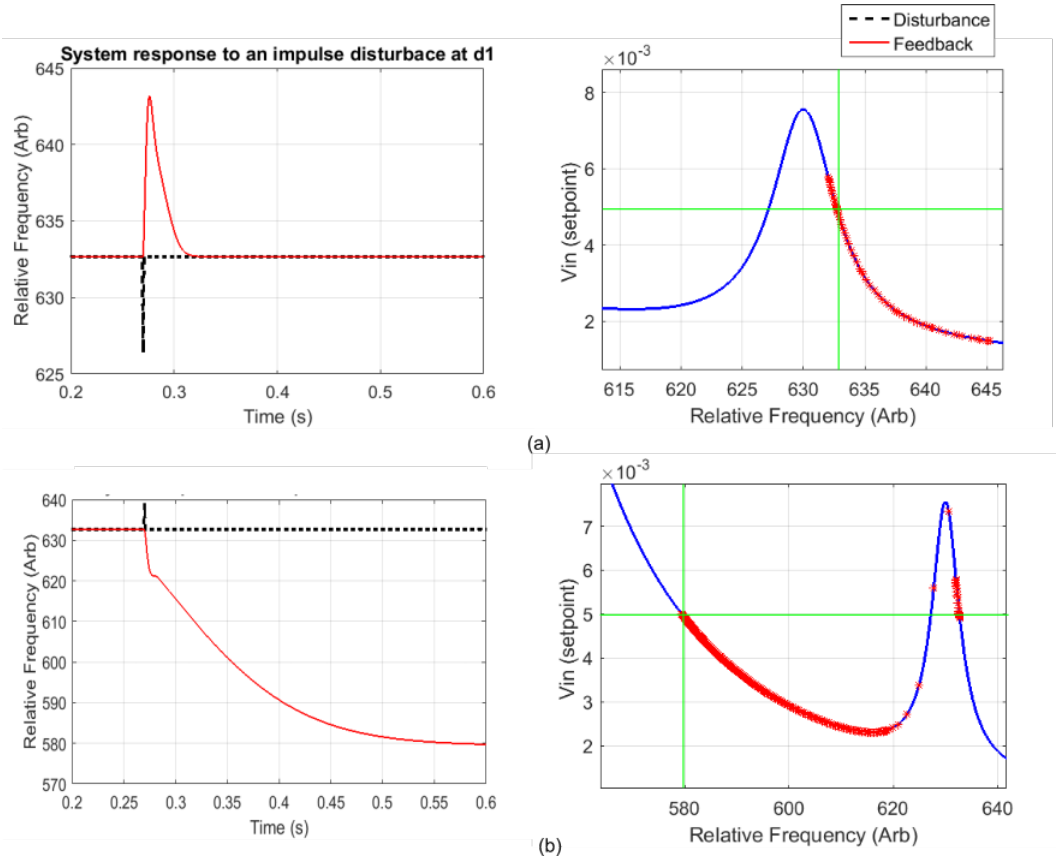

Figure 5.11: System response to impulse disturbance at d1. (a) shows the response for a positive step value and (b) for a negative step value

From figure 5.11 above, we notice that the system locks to the specified setpoint frequency (5.11(a)). We see a spike at $t = 0.3\ s$, but the system eventually settles to the chosen frequency. For a positive magnitude however, we observe that the system locks on to the chosen setpoint but on the wrong peak (peak **b** from figure 5.3). Thus a disturbance magnitude of that size at point **d1** 'shifts' the frequency

away from the chosen setpoint frequency to a different peak.

We apply the same impulse magnitude at point **d2** and the results are shown in figure 5.12.

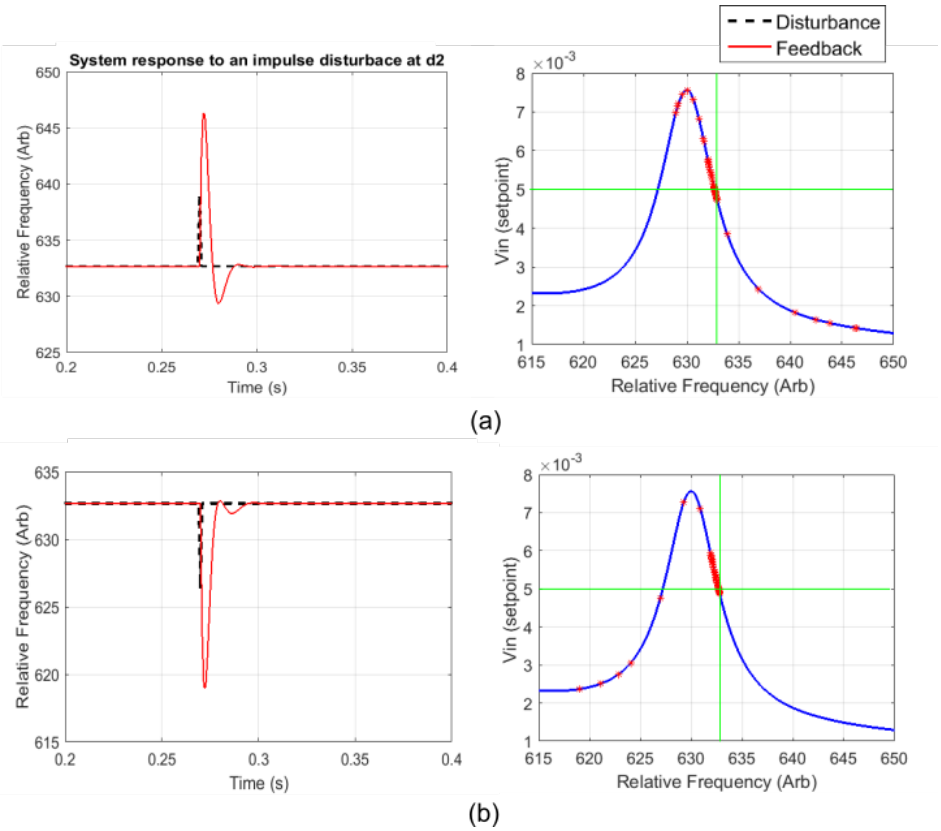

Figure 5.12: System response to impulse disturbance at **d2**. (a) shows the response for a positive step value and (b) for a negative step value

We observe from this figure that the system returns to the chosen setpoint frequency for both positive and negative step magnitudes of disturbance. Though the overshoot is larger for figure 5.12(a), they both have the same settling time (0.03 s). These values are summarised in table 5.3.

Table 5.3: System performance characteristics for impulse disturbance applied at d2

Parameters	**Plot (a)**	**Plot (b)**
Settling time (s)	0.03	0.03
Overshoot (%)	0.031	0.52

We again applied an impulse disturbance to point **d3** in the feedback system and the results are shown in figure 5.13.

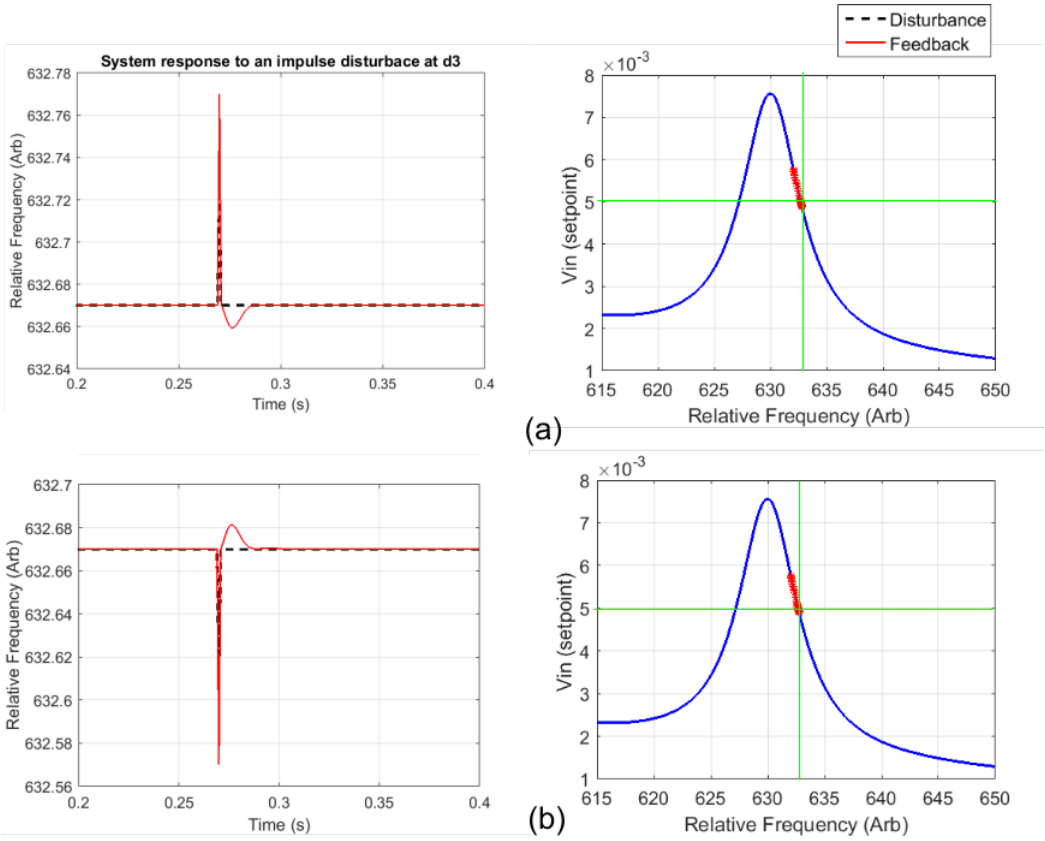

Figure 5.13: System response to impulse disturbance at **d3**

The results show that the disturbance has a very minimal effect of the feedback

system. They both have the same overshoot (0.0095 %) and settling time (0.03 s).

System response to a pulse disturbance

We further proceed to apply a pulse disturbance to **d1, d2, d3** using the same magnitude (0.1). We set it such that the width of the pulse was 50 ms. Figure 5.14, 5.15 and 5.16 shows the results.

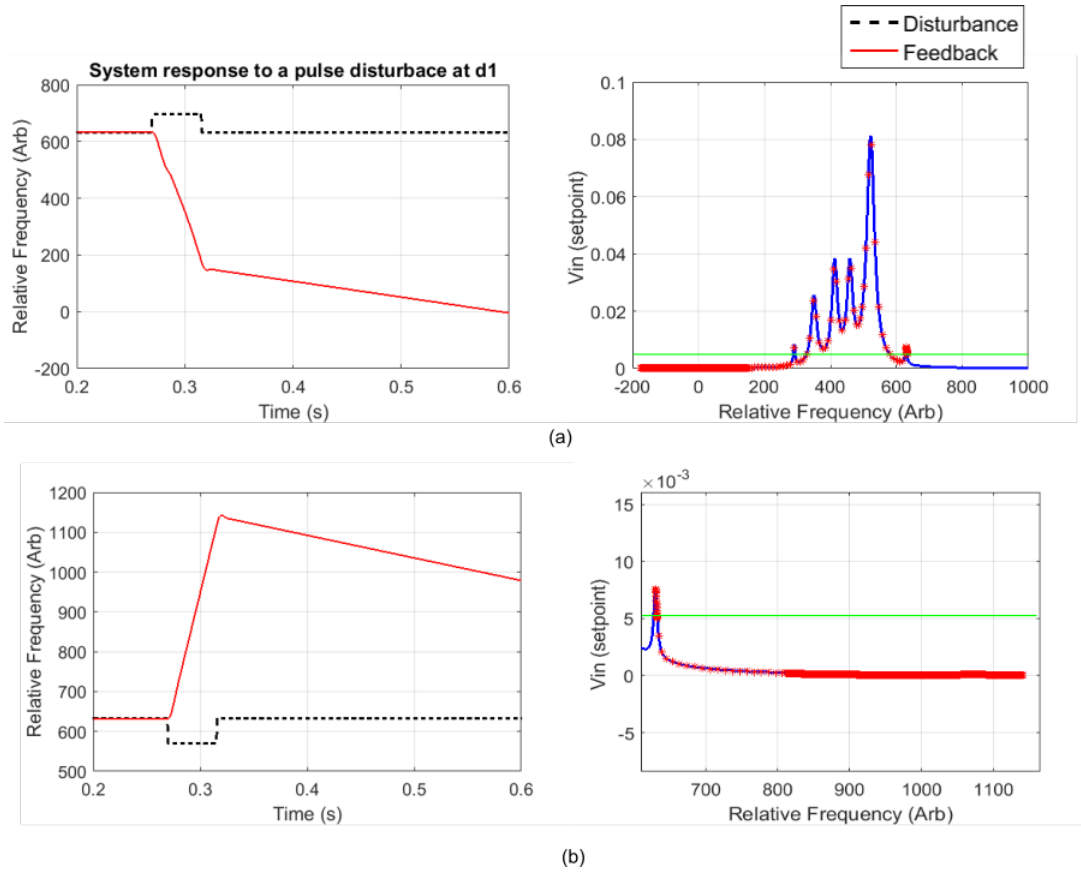

Figure 5.14: System response to a pulse disturbance at d1. (a) positive probe (b) negative probe disturbance.

From the figure 5.14 above, we observe that the system goes completely out of

lock. The magnitude of the pulse disturbance was simply too big for the feedback system to control.

Figure 5.15 shows the response of the system for disturbance at **d2**. We observe here that the system locks on to the wrong peak when a positive magnitude is added and locks to the right side of the curve for a negative magnitude. The overshoot is 1.32 % and has a settling time of 0.03 s

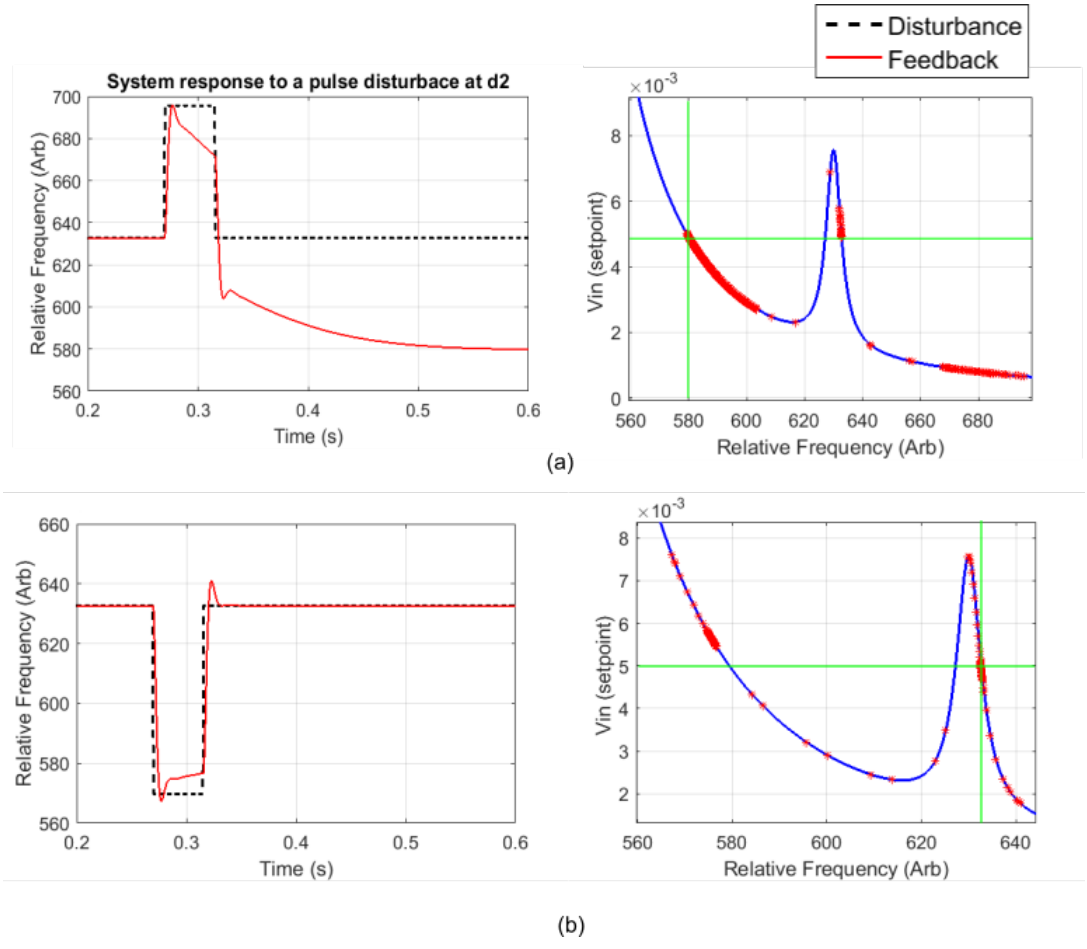

Figure 5.15: System response to a pulse disturbance at **d2**

Figure 5.16 shows that a pulse disturbance at **d3** has the least effect on the

feedback system, compared to results from **d2** and **d1**. The system locks at the appropriate transition for both disturbance scenarios (positive and negative magnitude).

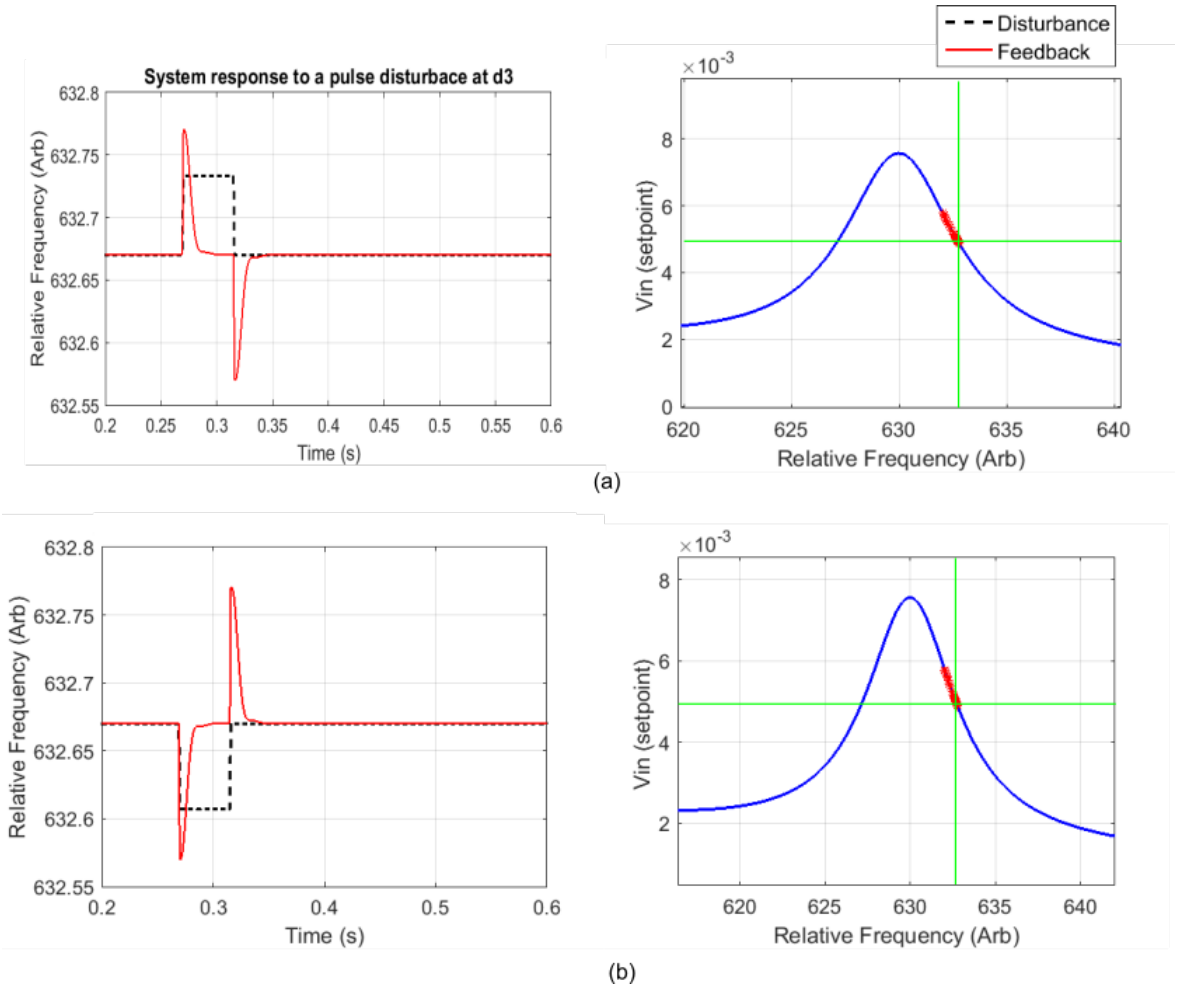

Figure 5.16: System response to a pulse disturbance at d3

From the numerical simulations, we can deduce that the system performs as desired. It is most sensitive to disturbances at **d1** and least sensitive at **d3**.

5.5 Summary

In this chapter, we have described how we numerically analysed the closed-loop feedback system for an external cavity diode laser (ECDL). We started by showing the overall system and then analysing each block numerically. We discussed how the ECDL was modelled mathematically, how we modelled the feedback setup using a series of Lorentzian functions derived from experimental results and how the PI controller was modelled using a gain and an integrator in form of a RC circuit. We also discussed the flow diagram for the software design, indicating how the program was developed in Matlab.

We further went on to discuss the results obtained from our simulations using extracted parameters from the experimental analysis chapter (chapter 4). We showed how the system responds to step changes, how the PI controller influenced the system by varying the different controller constants (K_p and τ) and how the system responds to different disturbance types.

Chapter 6

Summary and conclusion

In this thesis, we presented an experimental and numerical study of a closed-loop feedback control system for an external cavity diode laser (ECDL). This study provided key insight into the experimental setup and a framework to optimize the feedback system in the future.

We started by giving a detailed description of the feedback system's experimental setup was discussed. We showed the components currently being used in the laboratory to control the frequency of the ECDL.

We provided the theoretical background required to carry out this research. The concepts discussed includes control theory and basic physics concepts. The control theory covered includes feedback control theory and a detailed study of the performance and characterization of second order feedback control systems. Understanding this concept was crucial to our experimental analysis. For the

physics section, we covered the basics of laser-atom interactions and a gave detailed description of saturated absorption spectroscopy (SAS). SAS was discussed extensively because it is a core component of the laser locking setup. It acts as the feedback element in the control loop.

We went on to discuss how we experimentally analysed the feedback system. The operating modes and the steps taken to lock the ECDL frequency to a rubidium transition was also discussed. We further explained how we tested the system with test input signals to induce a transient response after locking the laser frequency. We further analysed the transient response to estimate the system parameters of the feedback system to obtain it's resonant frequency ω_n and damping constant ζ. Using these parameters, we were able to derive the transfer function of the system which was to be used in the numerical analysis.

We have also presented a numerical study of the feedback system. We showed how we used some parameters derived from our experiments to make the results as realistic as possible. We started by explaining how we modelled each component of the feedback system numerically and how the overall system was modelled in software. We further went on to discuss the results from our performance tests. Some of the results from the tests include the step response of the system for a step change in setpoint, the performance of the system to various controller constants (K_p and τ) and the feedback systems response to disturbances.

From the above, we conclude that we were able to meet the identified objectives required to complete this research. From our experiments, we observed the system was an underdamped system and behaved as a second order system.

The step response from our numerical simulation produced the desired result. It behaved as an underdamped system with minimal overshoot (0.06 %) and a short settling time (0.03 s). We also discovered the most disturbance-sensitive part of the closed-loop system to be the output from the feedback setup and the least sensitive part to be the input to the feedback curve.

Though the time scale and response time from both studies are similar, further work and more experiments can be taken to verify the accuracy of the numerical system. This can be considered for future work.

Another potential future work will be to perform a detailed analysis of the feedback system in Laplace domain. This will provide a model for comparative study and a possible avenue to verify the accuracy of our numerical model.

Appendices

Appendix A

Side Lock PID Controller

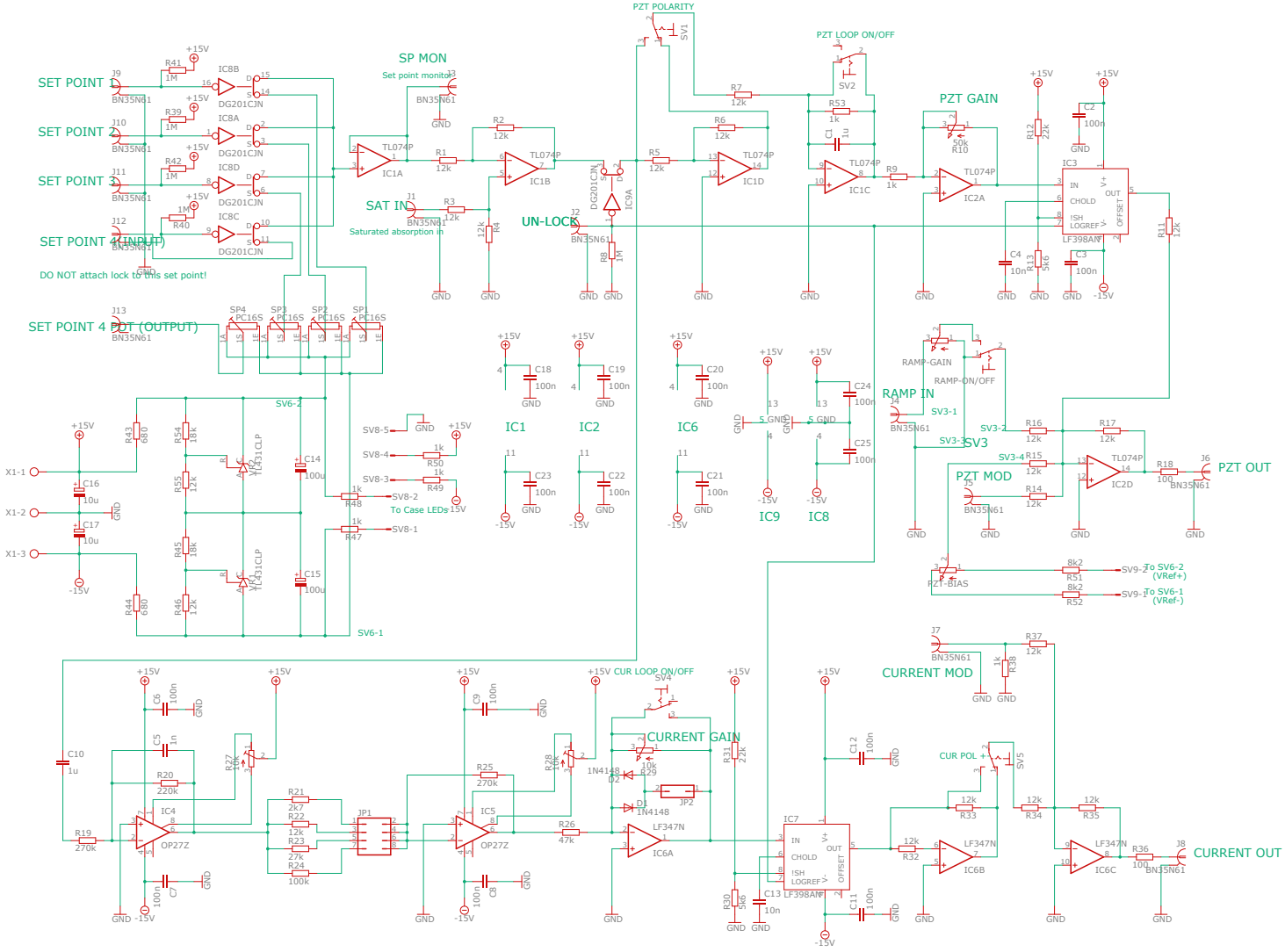

TITLE: Side Lock PID Controller v.12.0	
Document Number: 1 by Jordan Scarrott	REV:
Date: 24 Apr 2018 09:19	Sheet: 1/1

Appendix B

NI DAQ 6002 Specifications

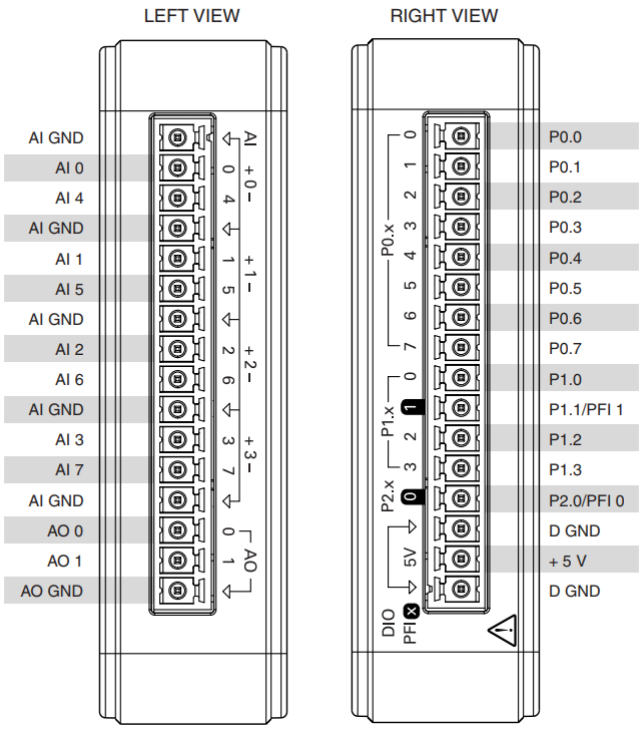

Figure B.1: NI-6002 Signal Description (*USER GUIDE - NI USB-6001/6002/6003* 2018)

References

Amr M., Ibrahim (2016). "Saturated Absorption Spectroscopy on Cs Atoms". Masters Thesis. Institute of Photonics, University of Eastern Finland.

Andrews, David L and David S Bradshaw (2016). "Laser cooling and trapping of atoms". *Optical Nanomanipulation*. 2053-2571. Morgan & Claypool Publishers, 4-1 to 4–5. ISBN: 978-1-6817-4465-0.

Bentley, J. P. (1995). "Principles of Measurement Systems". New York: Longman Scientific & technical, p. 163.

Blieck, J., X. Fléchard, A. Cassimi, H. Gilles, S. Girard, and D. Hennecart (2008). "A new magneto-optical trap-target recoil ion momentum spectroscopy apparatus for ion-atom collisions and trapped atom studies". *Review of Scientific Instruments* 79(10), p. 103102.

Bolton, W. (2018). *Mechatronics: Electronic Control Systems in Mechanical and Electrical Engineering*. 5th. Pearson Education, Limited.

Botha, G.N. (2009). "Development of an external cavity diode laser for application to spectroscopy and laser cooling and trapping of rubidium". Masters theses. Stellenbosch University.

Bowie, Jason, Jack Boyce, and Raymond Chiao (Oct. 1995). "Saturated-absorption spectroscopy of weak-field Zeeman splittings in rubidium". *J. Opt. Soc. Am. B* 12(10), pp. 1839–1842.

Burghes, D.N. and A. Graham (1980). *Introduction to control theory, including optimal control*. Ellis Horwood series in mathematics and its applications. E. Horwood. ISBN: 9780470269985.

Center, eCircuit (2004). *Op Amp PID Controller*. URL: `http://www.ecircuitcenter.com/Circuits/op_pid/op_pid.htm`.

Community, Electrical engineering (2014). *Typical Test Signals in Time Domain Analysis*. URL: `http://engineering.electrical-equipment.org/panel-building/typical-test-signals-in-time-domain-analysis.html`.

Corporation, Newport (2009). *TLB-6900 Vortex^{TM} II Series: Tunable External Cavity Diode Lasers*.

Cruse, H. (1996). *Neural Networks as Cybernetic Systems*. Thieme Publishers Series. G. Thieme Verlag.

Cunyun, Y. (2004). "Tunable External Cavity Diode Lasers". Texas: World Scientific Publishing Co., p. 4.

Debs, J. E., N. P. Robins, A. Lance, M. B. Kruger, and J. D. Close (Oct. 2008). "Piezo-locking a diode laser with saturated absorption spectroscopy". *Appl. Opt.* 47(28), pp. 5163–5166.

Dong, L., W. Yin, W. Ma, and S. Jia (2007). "A novel control system for automatically locking a diode laser frequency to a selected gas absorption line". *Measurement Science and Technology* 18, pp. 1447–1452.

Dorf, Richard C. and Robert H. Bishop (2000). *Modern Control Systems*. 11th. Upper Saddle River, NJ, USA: Prentice-Hall, Inc. ISBN: 0130306606.

Engelberg, Shlomo (2005). *A Mathematical Introduction to Control Theory*. 2nd. IMPERIAL COLLEGE PRESS.

Faizan, Ahmad (2018). *Transient Response — First and Second Order System Transient Response*. URL: `http://electricalacademia.com/control-systems/transient-response-analysis-and-system-stability-for-first-and-second-order-system/`.

Gawlik, W. and J. Zachorowski (2004). "Stabilization of diode-laser frequency to atomic transitions". *Optica Applicata* 34(4), pp. 607–618.

Gómez, J. F., J. J. Rosales, J. J. Bernal, and M. Guía** (2012). "Mathematical modelling of the mass-spring-damper system - A fractional calculus approach". *American Journal of Physics* 22(5), pp. 5–11.

Goodwin, Graham Clifford, Stefan F Graebe, Mario E Salgado, et al. (n.d.). *Control system design*. Vol. 240.

Grantham, Walter J. and Thomas L. Vincent (1993). *Modern Control Systems Analysis and Design: Analysis and Design*. 1st. New York, NY, USA: John Wiley & Sons, Inc. ISBN: 0471811939.

Gruska, Jozef (1999). *Quantum computing*. Vol. 2005. Citeseer.

Guiñón, J. L., Emma Ortega, Jose Maria Garcia-Anton, and Valentín Pérez-Herranz (2007). "Moving Average and Savitzki-Golay Smoothing Filters Using Mathcad".

Hale, F.J. (1973). *Introduction to Control System Analysis and Design*. Prentice-Hall. ISBN: 9780134798240.

Harvey, K. C. and C. J. Myatt (1991). "External-cavity diode laser using a grazing-incidence diffraction grating". *Canadian Journal of Physics* 16, pp. 910–912.

Hecht, E. (2013). *Optics*. Always learning. Pearson. ISBN: 9781292021577. URL: https://books.google.co.za/books?id=ZakzngEACAAJ.

Introduction: PID Controller Design (2017). URL: http://ctms.engin.umich.edu/CTMS/index.php?example=Introduction&section=ControlPID.

Jacques, V, B Hingant, A Allafort, M Pigeard, and J F Roch (2009). "Nonlinear spectroscopy of rubidium: an undergraduate experiment". *European Journal of Physics* 30(5), p. 921.

Jørgensen, N. B., D. Birkmose, K. Trelborg, L. Wacker, N. Winter, A. J. Hilliard, M. G. Bason, and J. J. Arlt (2016). "A simple laser locking system based on a field-programmable gate array". *Rev. Sci. Instrum.* 87(7), p. 073106.

Kassner, M. (2012). *How quantum cryptography works: And by the way, it's breakable*. URL: `http://techrepublic.com/blog/it-security/how-quantum-cryptographyworks-and-by-the-way-its-breakable`.

Kumar, Anupam and Vijay Kumar (Mar. 2017). "A novel interval type-2 fractional order fuzzy PID controller: Design, performance evaluation, and its optimal time domain tuning". *ISA transactions* 68.

Laurila, Toni, Timo Joutsenoja, Rolf Hernberg, and Markku Kuittinen (Sept. 2002). "Tunable external-cavity diode laser at 650 nm based on a transmission diffraction grating". *Appl. Opt.* 41(27), pp. 5632–5637.

Logeeswaran, V.J., F.E.H. Tay, M.L. Chan, F.S. Chau, and Y.C. Liang (Oct. 2003). "First Harmonic (2f) Characterisation of Resonant Frequency and Q-Factor of Micromechanical Transducers". *Analog Integrated Circuits and Signal Processing* 37(1), pp. 17–33.

Love, D. (2017). *'Quantum' technology is the future, and it's already here — here's what that means for you*. URL: `https://www.businessinsider.com/quantum-technology-2017-7?IR=T`.

MacAdam, K. B., A. Steinbach, and C. Wieman (1992). "A narrow-band tunable diode laser system with grating". *American Journal of Physics* 60(12), pp. 1098–1111.

Metcalf, Harold J. and Peter Straten (2007). "Laser Cooling and Trapping of Neutral Atoms". *The Optics Encyclopedia*. American Cancer Society.

Mongeau, Jean-Michel, Alican Demir, Chris J. Dallmann, Kaushik Jayaram, Noah J. Cowan, and Robert J. Full (2014). "Mechanical processing via passive dynamic properties of the cockroach antenna can facilitate control during rapid running". *Journal of Experimental Biology* 217(18), pp. 3333–3345. ISSN: 0022-0949.

Morari, M., M. Zafiriou, and E. Zafiriou (1989). *Robust Process Control*. Prentice Hall. ISBN: 9780137821532.

National Instruments (2018). *USB-6002 - Multifunction I/O Device*. URL: `http://www.ni.com/en-za/support/model.usb-6002.html`.

Nise, Norman S. (2011). *Control Systems Engineering*. 6th. New York, NY, USA: John Wiley & Sons, Inc.

Norris, I. (2009). "Laser Cooling and Trapping of Neutral Calcium Atoms". Ph.D. Department of Physics, University of Strathclyde.

Nyamuda, G.B. (2006). "Design and development of an extended cavity diode laser for laser cooling and spectroscopy applications". Masters theses. Stellenbosch University.

Papagiannopoulos, George and George Hatzigeorgiou (July 2011). "On the use of the half-power bandwidth method to estimate damping in building structures". *Soil Dynamics and Earthquake Engineering - SOIL DYNAM EARTHQUAKE ENG* 31, pp. 1075–1079.

Phillips, Charles L. and Royce D. Habor (1995). *Feedback Control Systems*. 4th. New York, NY, USA: Simon & Schuster, Inc. ISBN: 0133716910.

Preston, D.W. (1996). "Doppler-free saturated absorption: Laser spectroscopy". *American Journal of Physics* 64(11), pp. 1432–1436.

Rigby, Charles Ian (2011). "Development of a laser cooling and magneto-optical trapping experiment for rubidium 87 atoms". Masters theses. Stellenbosch University.

Salim, E. and H. Lewandowski (2012). *Laser Cooling and Trapping for Advanced Teaching Laboratories*. URL: massey.dur.ac.uk/resources/grad_skills/LaserCooling.pdf.

Saturated Absorption Spectroscopy using an ECDL (2017). URL: https://sites.google.com/a/umn.edu/mxp/advanced-experiments/saturated-absorption-spectroscopy.

Schwarzenbach, J. and K.F. Gill (1992). *System modelling and control*. 3rd. Edward Arnold.

Singh, J. (2008). *Quantum Mechanics: Fundamentals and Applications to Technology*. Wiley. ISBN: 9783527618200.

Steck, Daniel A. (2009). *Rubidium 87 D Line Data*. URL: `http://steck.us/alkalidata/rubidium87numbers.pdf`.

Stubbs, P.L. (2010). "Laser Locking with Doppler-free Saturated Absorption Spectroscopy".

Tehrani, Kambiz Arab and Augustin Mpanda (2012). "PID Control Theory". *Introduction to PID Controllers*. Ed. by Rames C. Panda. Rijeka: IntechOpen. Chap. 9.

Thorlabs, Inc. (2018). *Saturated Absorption Spectroscopy Systems*. URL: `https://www.thorlabs.com/newgrouppage9.cfm?objectgroup_id=5616`.

Traptilisa, F. (2014). "Characterization and Development of an Extended Cavity Tunable Laser Diode". Masters theses. San Jose State University.

USER GUIDE - NI USB-6001/6002/6003 (2018).

Weel, M. and A. Kumarakrishnan (2002). "Laser-frequency stabilization using a lock-in amplifier". *Canadian Journal of Physics* 80, pp. 1449–1458.

Wie, B., H. Weiss, and A. Arapostathis (1989). "Quarternion feedback regulator for spacecraft eigenaxis rotations". *Journal of Guidance, Control, and Dynamics* 12(3), pp. 375–380.

Wieman, Carl, Gwenn Flowers, and Gilbert Sarah (1995). "Inexpensive laser cooling and trapping experiment for undergraduate laboratories". *American Journal of Physics* 63(4), pp. 317–330.

Wyngaard, A. (2017). "Experimental Study of the Weak Field Zeeman Spectra of ^{85}Rb and ^{87}Rb".

Wyngaard, A.L. (2018). *Saturated Absorption Spectroscopy of Rubidium and Feedback Control of Laser Frequency for Doppler Cooling*. Cape Peninsula University of Technology.

Yahya, H. (2012). *The Solidity Of The Atom And Electron Orbits*. URL: `http://harunyahya.com/en/Miracles-of-the-Quran/151619/the-solidity-of-the-atom`.